JOURNAL OF GEOPHYSICAL RESEARCH, VOL. 106, NO. B3, PAGES 4305–4326, MARCH 10, 2001

Crustal velocity field of southwest Japan: Subduction and arc-arc collision

Shin'ichi Miyazaki

Geography and Crustal Dynamics Research Center, Geographical Survey Institute
Tsukuba, Japan

Kosuke Heki

Division of Earth Rotation, Mizusawa Astrogeodynamics Observatory
National Astronomical Observatory, Mizusawa, Japan

Abstract. We investigate crustal deformation in southwest Japan over a 3-year period revealed by a permanent dense Global Positioning System (GPS) array. Southwest Japan is a part of the Amurian Plate, a microplate moving about 10 mm/yr toward the east with respect to the Eurasian Plate. It overrides the Philippine Sea Plate at the Nankai Trough and collides with the northeast Japan arc in the central part of Japan. In this paper we first derive GPS site velocities relative to the stable part of the Amurian Plate in order to isolate signals of crustal deformation caused by the subduction and/or the collision. The velocity field has a conspicuous feature indicating the interseismic elastic loading by the Philippine Sea Plate slab at the Nankai Trough, characterized by the northwestward movements of points throughout the studied area. Their amplitudes are the largest at the Pacific coast and decay toward the Japan Sea coast with a subtle systematic shift of azimuths. A model assuming an elastic half-space, the convergence rate at the Nankai Trough based on a refined Euler vector, and the strength of the coupling inferred from a thermal model, could explain the velocity field in the western part of the studied area to a large extent. Those in the eastern part systematically deviate from them, and the residual components there show east-west shortening and north-south extension. This may represent crustal thickening and trenchward extrusion of crustal blocks caused by the collision between southwest and northeast Japan. This suggests that the collision between southwest and northeast Japan gives rise to not only crustal thickening but also trenchward extrusion of crustal block. A velocity contrast was found across the Median Tectonic Line, the largest inland active fault in Japan, but the current permanent GPS network is not dense enough for us to discuss its coupling depth.

1. Introduction

Interseismic crustal deformation in southwest Japan is dominated by its interaction with the Philippine Sea Plate (PH) that subducts at the Nankai Trough, off Shikoku island and the Kii Peninsula (Figure 1). Historic records of large thrust earthquakes at the Nankai Trough available for over 1000 years suggest the recurrence interval of 100-200 years [*Ando*, 1975; *Sangawa*, 1993; *Kumagai*, 1996], and the 1944 Tonankai and the 1946 Nankaido earthquakes are the latest of such events. Terrestrial geodetic surveys have been performed by the Geographical Survey Institute (GSI) of Japan for more than one century, and such data have revealed interseismic crustal deformation [*Hashimoto*, 1990; *Hashimoto and Jackson*, 1993; *Ishikawa and Hashimoto*, 1999]. Those geodetic results recorded coseismic jumps from time to time, which were used to infer the distribution of fault slips at depth. For example, slip distributions associated with the 1944 and 1946 events were estimated using such data by several researchers [e.g., *Yabuki and Matsu'ura*, 1992; *Sagiya and Thatcher*, 1999].

Past geodetic and seismological studies helped us constrain the downdip extent of the seismogenic zone in the Nankai Trough. In 1994 GSI started to establish a nationwide permanent array of Global Positioning System (GPS) stations called GPS Earth Observation Network (GEONET) [*Miyazaki et al.*, 1997; *Kato et al.*, 1998a]. This network has provided significant new information on crustal deformation in Japan. For example, interseismic crustal deformation in southwest Japan has

Paper number 2000JB900312.
0148-0227/01/2000JB900312$09.00

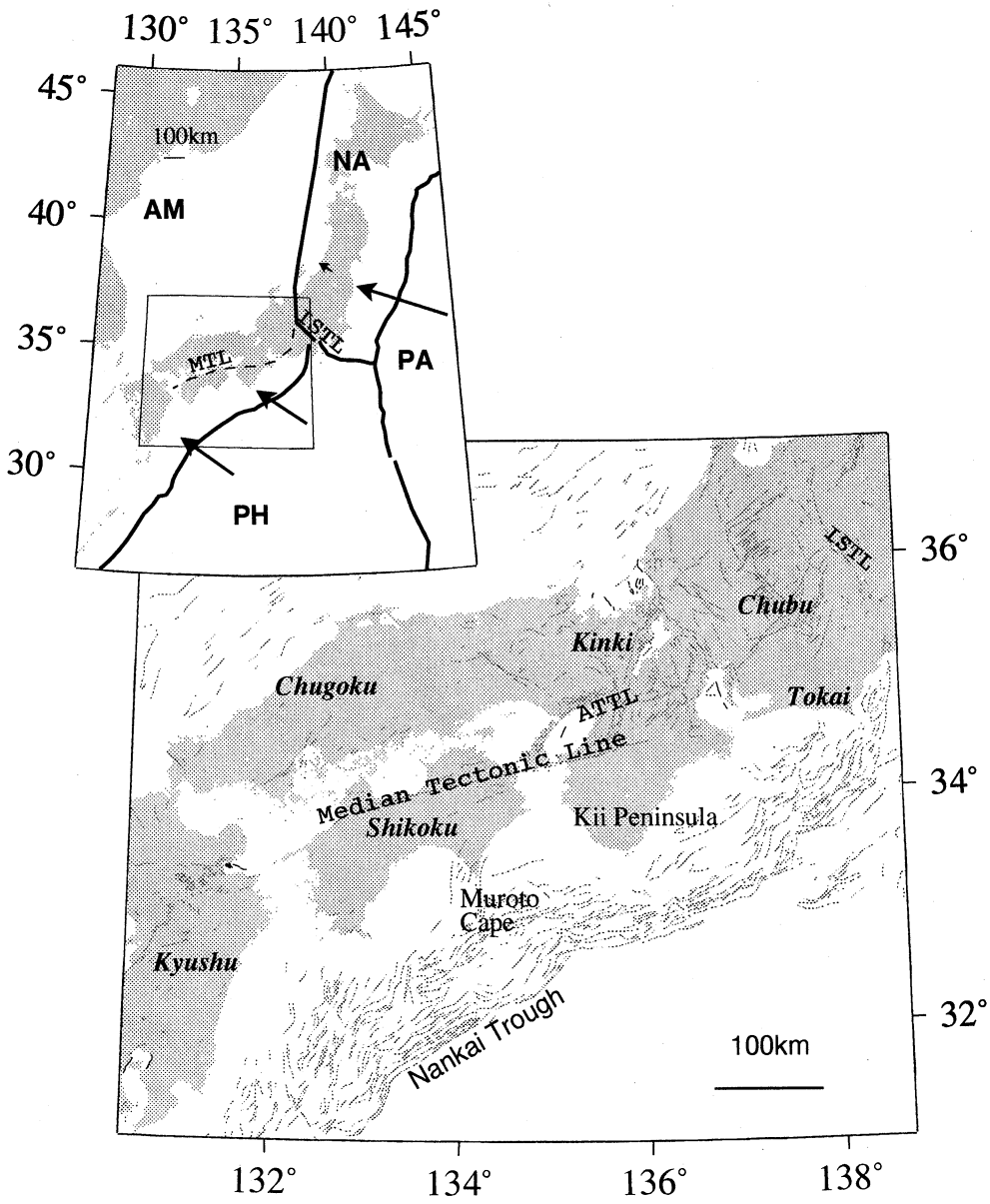

Figure 1. Tectonic setting of the Japanese islands. Southwest Japan, a part of the Amurian Plate (AM), is overriding the Philippine Sea Plate (PH) at the Nankai Trough and is possibly colliding with northeast Japan along the Itoigawa-Shizuoka Tectonic Line (ISTL) in the central Japan. The Median Tectonic Line (MTL), which is a right-lateral strike-slip fault, runs from the ISTL through Chubu district, Kii Peninsula, and Shikoku district. The northern and southern sides of the MTL are often referred to as the inner and the outer zones, respectively. Abbreviations NA, North American Plate; PA, Pacific Plate; ATTL, Arima-Takatsuki Tectonic Line.

been studied by *Ozawa et al.* [1999], *Ito et al.* [1999], and *Mazzotti et al.* [2000]. They modeled crustal deformation with interseismic coupling between island arc lithosphere and the Philippine Sea slab. However, as will be discussed later, these studies have problems in choosing kinematic reference frames.

Seno et al. [1993] estimated the relative rotation (Euler) vector of PH using slip direction data of interplate earthquakes along the Nankai Trough assuming that they represent the convergence direction between PH and the Eurasian Plate (EU). In past studies with GPS data, southwest Japan has also been regarded as a part of EU, that is, interseismic velocities have been converted to those with respect to the stable interior of EU in order to study crustal deformation there [e.g., *Kato et al.*, 1998a]. Figure 2 shows the interseismic velocity field relative to EU obtained from 3 years of continuous observations (the velocity uncertainties are evaluated but not shown here; see section 3 for details). Velocity field relative to EU has been modeled assuming interseismic elastic loading of the island arc by the slabs along the Nankai Trough [e.g., *Mazzotti et al.*, 2000].

GPS sites in the Chugoku district are moving eastward fairly coherently by about 10 mm/yr. Needless to say, such systematic eastward velocities cannot be explained by the subduction.

Although interseismic velocity field in southwest Japan is dominated by the crustal deformation caused by the PH subduction, crustal stress in this region is characterized by the compression in a significantly different direction from the subduction. This apparent inconsistency between the stress and the strain rates, along with the eastward movement of the inner arc, suggest complicated nature and multiple origins of crustal deformation in southwest Japan.

In this paper we present geophysical interpretation of the GEONET GPS site velocity field in southwest Japan as seen in Figure 2. The following two problems seem to make this task difficult, that is, (1) selection of the kinematic reference frame and (2) coexistence of two different crustal deformation sources, the subduction at the Nankai Trough to the south and the collision with northeast Japan to the east. In the next section we summarize strategies to overcome these problems.

2. Analysis Strategy

2.1. Kinematic Reference Frame

Proper interpretation of interseismic crustal deformation of an island arc is facilitated by the use of a kinematic reference frame fixed to the stable interior of the landward plate. When such a frame is not available, we instead rely on quantities that do not require reference frames, such as crustal strain rates [*Mazzotti et al.*, 2000] and baseline length changing rates [*Ito et al.*, 1999]. Actually, it is changes in velocities that constrain the strain accumulation models, but such an approach often suffers from poor signal-to-noise ratio when the spatial coverage of the site distribution is small and intersite movements are slow. The kinematic reference frame fixed to the stable interior enables us to use the velocity values themselves (which are movements "relative to" the stationary plate interior) without making differences and usually offers better constraints to the model. It would be from this point of view that *Ozawa et al.* [1999] fixed a GPS site on the Japan Sea coast of the Chugoku district, the farthest point from the plate

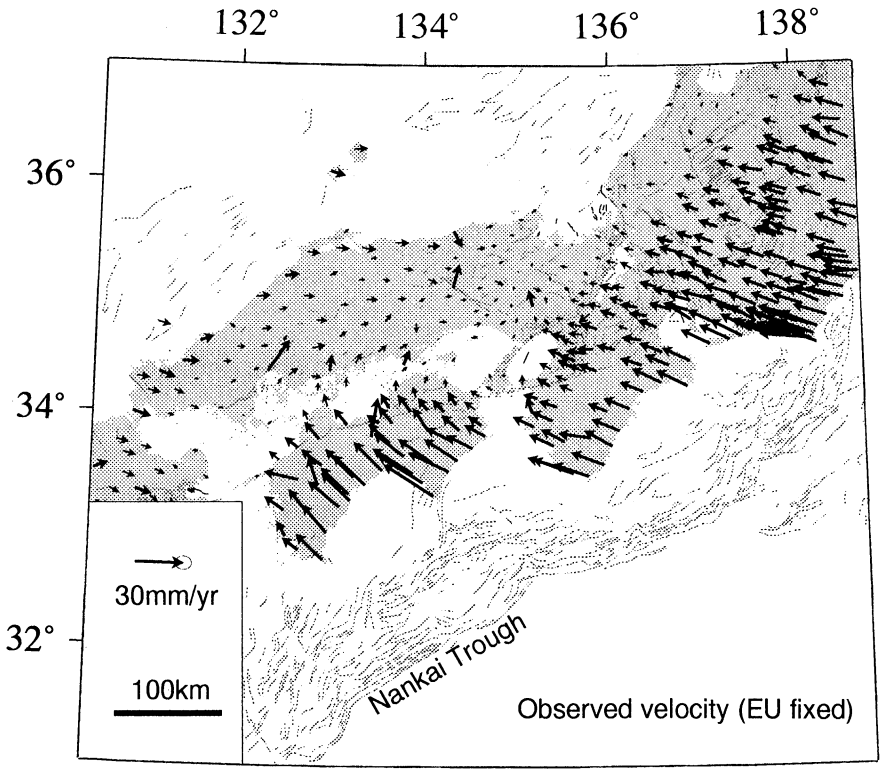

Figure 2. The interseismic crustal velocity field of southwest Japan with respect to the stable interior of the Eurasian Plate. Velocity uncertainties are omitted for clarity. Typical velocity uncertainties for sites observed for 3 years (2.1 and 1.7 mm/yr for the east and north components, respectively) are shown in the legend. Site velocities in the Chugoku district reveal significant eastward movement of 5-10 mm/yr, consistent with Amurian Plate motion. The velocity field in the Shikoku district shows northwestward movement, mostly elastic response of subduction at the Nankai Trough. Several outliers are found to be due to the monument instabilities.

boundary, in order to estimate the back slip distribution [*Savage*, 1983] on the plate interface.

The tectonics of central and eastern Asia is characterized by two major factors, subduction of oceanic lithospheres along the eastern and southeastern coast and eastward expulsion of relatively small continental blocks caused by the collision of India with Eurasia [*Molnar and Tapponnier*, 1975]. Based on regional tectonics and seismicity, *Zonenshain and Savostin* [1981] proposed the existence of one such plate, the Amurian Plate (AM), covering northeast China, the Korean Peninsula, the Japan Sea, and the southeastern part of Russia. Recently, *Heki et al.* [1999] analyzed data from several continuous GPS observation sites considered to be on the stable interior of AM. They found that those sites move eastward with respect to EU by about 10 mm/yr but are stationary with respect to one another. They estimated the EU-AM Euler vector and suggested that southwest Japan is the southeasternmost part of AM and the eastward movements there come from its movement relative to EU. They also showed that by switching the kinematic reference frame from EU to AM, eastward GPS velocities in southwest Japan change to northwestward [see *Heki et al.*, 1999, Figure 5]. This suggests that elastic straining due to the AM-PH plate convergence extends as far northwest as the Japan Sea coast of the Chugoku district causing a few mm/yr movements even at the farthest points from the trough. Therefore fixing a certain site in southwest Japan [*Ozawa et al.*, 1999] is not appropriate for the present purpose. In this paper we follow *Heki et al.* [1999] and fix the kinematic reference frame to AM by using their new Euler vector.

2.2. Two Modes of Crustal Deformation in Southwest Japan

While interseismic crustal deformation in southwest Japan is dominated by the NW-SE contraction caused by the subduction of PH (Figure 2), the maximum horizontal stress axis is nearly E-W. This can be seen in the *P* axis directions of inland crustal earthquakes in southwest Japan including those in the southern Shikoku [*Okano et al.*, 1985] where NW-SE shortening rate is the largest. Such inland earthquakes include the 1995 Hyogoken-Nanbu earthquake as indicated by the focal mechanism solution showing E-W compression [*Kikuchi and Kanamori*, 1996; *Hashimoto et al.*, 1996]. *Wang* [2000] pointed out that the interseismic NW-SE crustal shortening arises from plate coupling at the Nankai Trough, while E-W compression comes from the broader scale plate tectonic setting of the region. He suggested that this apparent stress-strain rate "paradox" stems from the misunderstanding of what these data indicate, that is, the earthquakes indicate stress level while geodetic data indicate only the changes of crustal strains during the measured period. This suggests that although instantaneous crustal strain changes are dominated by the interseismic elastic loading by the slab, stress level in this direction is much lower than the E-W component possibly caused by the collision between the two island arcs.

There have been arguments concerning the origin of this E-W compression. *Huzita* [1980] attributed it to the subduction of the Pacific Plate (PA) at the Japan Trench. Later, *Kobayashi* [1983] and *Nakamura* [1983] simultaneously hypothesized that a newly born plate boundary runs along the eastern margin of the Japan Sea and the Itoigawa-Shizuoka Tectonic Line (ISTL), across central Japan down to the Pacific coast (Figure 1). They inferred that the North American Plate (NA)-EU convergence along this boundary is responsible for the E-W compression in central Japan. Later, *Ishibashi* [1995] emphasized the importance of the eastward movement of southwest Japan as the cause of the E-W compression and suggested this movement is due to the eastward motion of AM. *Heki et al.* [1999] supported this view that southwest Japan, a part of AM, moves eastward and collides with northeast Japan causing E-W compression. Such a strong E-W compressional stress would cause large permanent crustal shortening in the long run, while most of the rapidly accumulating NW-SE shortening would disappear when the next interplate earthquake occurs in the Nankai Trough.

The ISTL geologically divides southwest and northeast Japan, and the convergence between the arcs has been considered to occur along this narrow zone. However, terrestrial geodetic survey results [*Hashimoto*, 1990; *Ishikawa and Hashimoto*, 1999] did not show significant E-W shortening along this line. *Hashimoto and Jackson* [1993] modeled crustal deformation in Japan with a block fault model and found that significant E-W shortening takes place also in several tectonic lines in the Kinki and Chubu districts other than ISTL [see *Hashimoto and Jackson*, 1993, Figure 7]. Their result implies the collisional deformation is accommodated by a diffuse zone whose eastern limit nearly coincides with ISTL. These considerations suggest that the crustal deformation in southwest Japan consists of two components; the first component caused by the subduction of PH and the second component caused by its collision with northeast Japan. It is not straightforward to discriminate these components because they are not orthogonal to each other. In order to isolate either one of the components, we can, for example, introduce a certain a priori model of the other (the one whose mechanism is better understood). In this paper we model the crustal deformation due to the subduction so that we can isolate the collisional deformation out of the observed velocity field.

3. Velocity Data

GEONET currently consists of 949 permanent sites; 210 of them started operation as the first generation sites of the predecessor network of GEONET

in the South Kanto and Tokai districts (Continuous strain monitoring observation system with GPS by GSI (COSMOS-G2)) in April 1994 and in the whole nation (GPS regional array for precise surveying (Grapes)) in October 1994 [*Tsuji et al.*, 1995]. The number of sites became 610 in April 1996, and 276 and 60 sites were further added in June 1997 and April 1998, respectively. We use a 3-year record of the GEONET solutions for the 610 sites and use 2-year solutions for the 276 sites, to investigate crustal deformation in southwest Japan. The network configuration and analysis strategy of the daily processing are described by *Miyazaki et al.* [1997]. Here we briefly summarize the outline.

Since the network has many points, we divide it into three subnetworks based on antenna-receiver types for the baseline analysis. In order to keep the antenna-receiver types homogeneous, these subnetworks do not have common stations to tie them. However, every subnetwork has a station within 100 m range from Tsukuba International GPS Service (IGS) (TSKB) station (TKBA for Ashtech, 2110 for Trimble, TKB4 for Leica subnetwork), whose coordinates are estimated in International Terrestrial Reference Frame (ITRF96) by a simple baseline processing with TSKB before the whole network processing. Each subnetwork is further divided into clusters and subordinate units. Ionosphere-free linear combinations of the L1 and L2 phase observables are processed using the Bernese software version 4.1β, the developing version used in University of Bern (J. Johnson and M. Rothacher, personal communication, 1996), precise orbit information provided by the IGS and the Earth rotation parameters from the International Earth Rotation Service Bulletin B. The orbit and the Earth rotation parameters are fixed to the a priori values. Tropospheric zenith delays are estimated for every 3-hour interval. Normal equations for all clusters are combined to estimate site positions imposing a tight constraint on the coordinates of TKBA, 2110, and TKB4 sites for the Ashtech, Trimble, and Leica subnetworks, respectively. Solutions between different subnetworks are therefore uncorrelated. Tsukuba station of one particular subnetwork (2110) was found to suffer from monument instability of about 1 cm, which introduced a constant bias in the time series of all the sites of Trimble subnetwork. Hence we analyzed the baseline between the fiducial site (TKBA, 2110, TKB4) of each subnetwork and the TSKB station and added the independent correction term to each subnetwork to obtain the consistent velocity solution.

Site velocities are estimated from the daily estimates of coordinates. Changes of the site coordinates consist of a linear trend, seasonal variation, seismic crustal deformations, and so on. In this study, time series are modeled as the sum of the constant secular velocity terms, trigonometric functions with biannual and annual periods, and coseismic jumps associated with earthquakes during the analyzed periods. Variations other than linear trends are estimated simultaneously with the robust estimation method developed by *D. Dong* (QOCA (Quasi-Observation Combination Analysis), http://sideshow.jpl.nasa.gov:80/~dong/qoca/, Jet Propul. Lab., Pasadena, Calif., 1999). In this study we discuss only the linear trends, which represent interseismic crustal deformation in Japan. Several relatively large interplate earthquakes occurred off the Kyushu district at the Nankai Trough on October 18, 1996 ($M_{JMA} = 6.6$), October 19, 1996 ($M_{JMA} = 6.6$), and December 3, 1996 ($M_{JMA} = 6.6$), and significant long-term postseismic deformations similar to the 1994 Sanriku-Haruka-Oki Earthquake [*Heki et al.*, 1997] were found in the GEONET GPS records [*Nishimura et al.*, 1999]. In addition to the afterslip, *Hirose et al.* [1999] reported that a "slow thrust slip (STS) event," an interplate thrust event without any sizable earthquakes, occurred just west of the studied area and lasted over 1 year from December 1996. The velocity field in Kyushu might be affected by these transient phenomena and were not used in the present study.

We fix the kinematic reference frame to AM by the following procedure. The original velocity field is in the ITRF96 system [*Sillard et al.*, 1998]. This frame consists of station positions and velocities, and its kinematic part (i.e., velocity field) is intrinsically aligned to the nnr-NUVEL1a model [*Argus and Gordon*, 1991; *DeMets et al.*, 1994]. In principle, velocities relative to EU could be obtained by subtracting the absolute rotation of EU predicted by the model. These EU-fixed velocities were then converted to those with respect to AM using the AM-EU Euler vector given by *Heki et al.* [1999].

Zhang et al. [1997] and *Mao et al.* [1999] suggested that errors in GPS time series consist of white noise components and colored components that arise from unmodeled effects in the baseline analysis procedure such as tropospheric delay gradients, multipath, and monument instabilities. Although time spans discussed in their studies are not long enough to estimate the random walk parameters, they concluded that a combination of white noise and flicker noise better characterizes the noise behaviors of the site coordinates than that of white noise and random walk. In our study, velocity uncertainties are evaluated assuming such flicker noise as well as white noise. *Mao et al.* [1999] gave an approximate expression for the total rate error that is valid for evenly spaced measurements as

$$\sigma_r = \left[\frac{12\sigma_w^2}{gT^3} + \frac{a\sigma_f^2}{g^b T^2} \right]^{1/2}, \qquad (1)$$

where g is the number of measurements per year, T is the total time span in years, σ_w and σ_f are the magnitudes of white and flicker noise in millimeters, respectively, and a and b are constants empirically estimated as $a \sim 1.78$ and $b \sim 0.22$ (random walk component is neglected here). *Mao et al.* [1999] analyzed 3-year time

series, the same time span as our data sets, and found the magnitude of flicker noise (σ_f) is 7.1 ± 2.8 mm for north and 9.0 ± 2.4 mm for east components for sites located in regions other than North America, western Europe and the tropical zone (between $-23°$ and $23°$ in latitude). Since *Mao et al.* [1999] did not recognize significant correlation between the magnitudes of white and flicker noise components, we used the mean values as the amplitude of flicker noises for all sites and roughly evaluated its contribution taking time spans into account using the above formula. The error estimated for sites observed for 3 years is 2.1 mm/yr (east) and 1.7 mm/yr (north), and 3.2 mm/yr (east) and 2.5 mm/yr (north) for those observed for 2 years. Recently, *Dixon et al.* [2000] pointed out that errors given by *Mao et al.* [1999] may be too conservative for more modern analyses or different site locations. They proposed to use weighted-root-mean-squares (WRMS) to estimate the magnitude of white/flicker noise based on the correlation between WRMS and such noise. We followed this method and obtained the revised estimate of the mean velocity errors of 0.6 and 0.5 mm/yr for east and north components, respectively.

Velocity errors should take account of frame-origin errors as well as those derived in time-series analyses. *Heki et al.* [1999] compared site velocities at Tsukuba, Japan and Shanghai, China, derived by GPS and very long baseline interferometry (VLBI) [*Heki*, 1996], and suggested that the error coming from the reference frame inconsistency would not exceed 1.1 mm/yr in eastern Asia. The conversion of the kinematic reference frame from EU-fixed to AM-fixed would also add small amount of error, and the formal error of the AM-EU Euler vector by *Heki et al.* [1999] predicts it to be 0.7-0.8 mm/yr in southwest Japan. In this study we adopt the errors based on *Mao et al.* [1999] given in the previous paragraph as the nominal ones, which are thought to be conservative enough even after taking the frame definition errors into account.

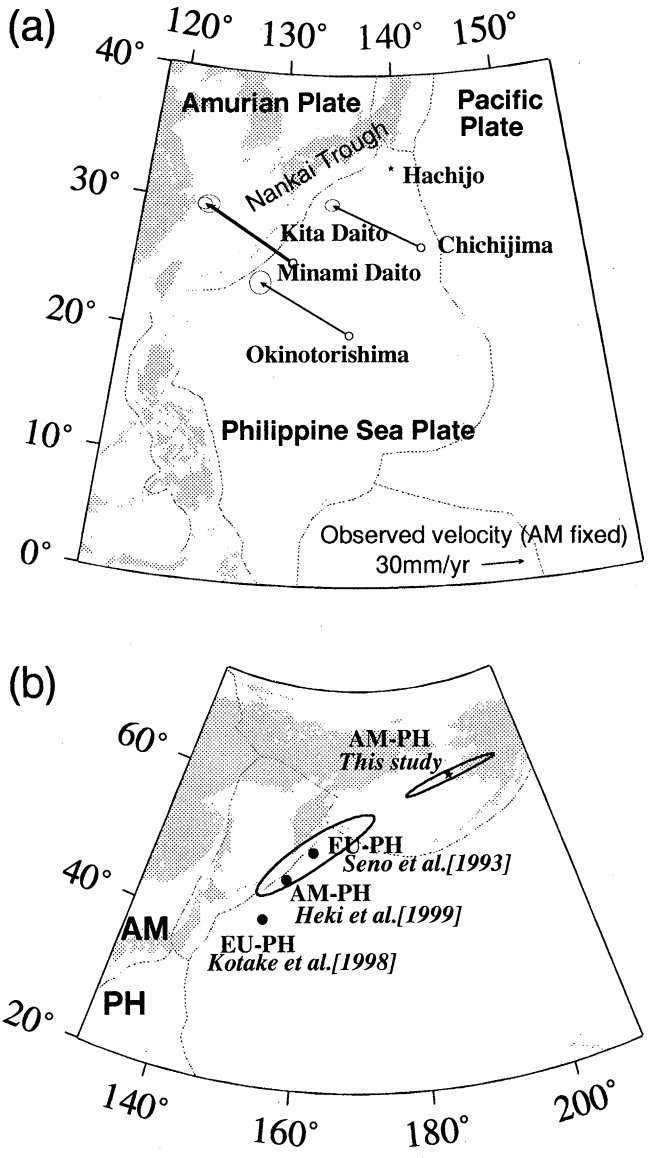

Figure 3. (a) GPS site velocities used to determine the relative movement of the Philippine Sea Plate. GPS observations at Okinotorishima (Palace Vela) are campaign based but span a 4-year period. Other sites are the part of GEONET, whose observation period is 3 years. We did not use observations at Hachijo because it is an active volcanic island whose velocity may be affected by magma chamber inflation.
(b) Estimated positions of the AM-PH and EU-PH Euler poles from this and other recent studies. Error ellipses are 2σ (95% confidence).

4. Redetermination of the Philippine Sea Plate Movement

In order to discuss crustal deformation caused by the subduction, it is important to precisely know the AM-PH relative movement at the Nankai Trough. It has been relatively difficult to determine the Euler vector of PH since the plate is surrounded mostly by convergent boundaries. For example, *Seno et al.* [1993] determined the PH Euler vector relying on the earthquake slip vectors and the circuit closure of plate kinematics. However, their Euler vector might be influenced by wrongly assuming the Nankai Trough as the EU-PH boundary (it actually is the AM-PH boundary). The problem is further complicated by local-scale crustal deformation, for example, active back arc spreading at the Okinawa Trough and the Mariana Trough. Hence using site velocity data by direct space geodetic measurements would be a meaningful step to improve the PH Euler vector.

Kotake et al. [1998] estimated the EU-PH Euler vector by using GPS site velocities at four islands, Okinotorishima (Palace Vela), Minami-Daito, Hachijo, and Chichijima islands (Figure 3a). The Okinotorishima GPS site is campaign based but its observing time span is long enough (4 years) to derive an accu-

Table 1a. GPS Data Used in the Euler Vector Estimation and Postfit Velocity Residuals

GPS Station	Position		Velocity		Velocity Uncertainty[a]		Data Residual	
	Longitude, deg	Latitude, deg	East, mm/yr	North, mm/yr	East, mm/yr	North, mm/yr	East, mm/yr	North, mm/yr
Okino-Torishima	136.1	20.4	-63.0	37.6	3.3	3.1	0.7	4.0
Chichijima	142.2	27.1	-60.8	33.1	1.7	2.1	-0.8	-2.1
Minami-Daito	131.2	25.8	-63.7	39.8	1.7	2.1	0.9	-0.6
Kita-Daito	131.3	26.0	-61.3	38.4	2.5	3.2	-0.5	1.7

[a] One standard deviation.

rate velocity estimate. Other sites belong to GEONET and their velocities are based on the observations of only 1 year. *Heki et al.* [1999] calculated the AM-PH Euler vector by combining their AM-EU vector with the EU-PH vector of *Kotake et al.* [1998]. Small but systematic differences were found by *Kotake et al.* [1998] between the predicted convergence directions and the earthquake slip vectors observed at the Nankai-Ryukyu Trough. The misfits become smaller by using the AM-PH Euler vector by *Heki et al.* [1999] but still seem systematic.

In this study we revise the AM-PH Euler vector using new velocity data of the GEONET GPS points (Minami-Daito, Kita-Daito, and Chichijima) using data spanning 3 years. We use the same velocity of Okinotorishima as given by *Kotake et al.* [1998] (see Figure 3a). We did not use the velocity of the Hachijo island, an active volcanic island where the velocity might be affected by the inflation of the magma chamber between eruptions. Site velocities are first converted to those relative to AM, then we estimated the AM-PH Euler vector using the weighted least square method. The result is summarized in Tables 1a and 1b and plotted in Figure 3b. The WRMS of the postfit velocity residuals was 1.5 mm/yr, suggesting that the area covered by these GPS points is fairly rigid. Errors given in Table 1b shows that the Euler pole position was strongly constrained even without the velocity of Hachijo. This Euler vector predicts the AM-PH convergence at the Nankai Trough of 63-68 mm/yr toward $\sim$ N55W.

We compare slip directions predicted by our new Euler pole with earthquake slip vectors at the Izu-Bonin Trench and the Nankai-Ryukyu Trough listed by *Seno et al.* [1993]. Figure 4a compares those at the Izu-Bonin trench. Predicted directions are shown both for the EU-PH Euler pole of *Seno et al.* [1993] and for the AM-PH poles of the present study. The WRMS of angular residuals, calculated using the observation errors given by *Seno et al.* [1993], is 5.3°, which is much smaller than the typical observation errors of 10 $\sim$ 20° [*Seno et al.*, 1993]. Figure 4b compares those along the Nankai-Ryukyu Trough. The WRMS of 7.2° for the present result and 6.5° for *Heki et al.* [1999] are within the observational uncertainties. The slight increase of the WRMS for our Euler vector is due to large deviations of two earthquakes at the Ryukyu Trough, and the WRMS decreases to 5.2° without these data. The following two reasons suggest that slip vectors at the Ryukyu Trench may not represent the AM-PH relative movement. First, the lithosphere south of the Qinling Fault, China, is considered to be the South China block, another crustal block moving eastward slightly faster than AM [*Heki et al.*, 1999]. Second, the back arc spreading at the Okinawa Trough [e.g., *Tada*, 1984, 1985] may affect the slip direction. *Sibuet et al.* [1998] suggested that the rifting direction is nearly perpendicular to the trough around the main Ryukyu island but nearly north-south in the southwestern part. This would deflect the convergence direction between PH and the southwestern Ryukyu islands clockwise.

Table 1b. Euler Pole Positions and Rotation Rates Estimated Using GPS Data

Plate Pair	Pole		Angular Rate		Error Ellipse		
	Latitude, deg	Longitude, deg	ω, deg/Ma	σ_ω, deg/Ma	σ_{max}, deg	σ_{min}, deg	ζ_{max},[a] deg
AM-PH[b]	61.0	191.2	0.83	0.07	5.7	0.6	72.6
EU-PH[c]	51.0	160.6	1.19	0.50	9.1	1.9	50.0

[a] Variable ζ_{max} is the azimuth of the maximum axis measured clockwise from north.

[b] This study.

[c] *Seno et al.* [1993].

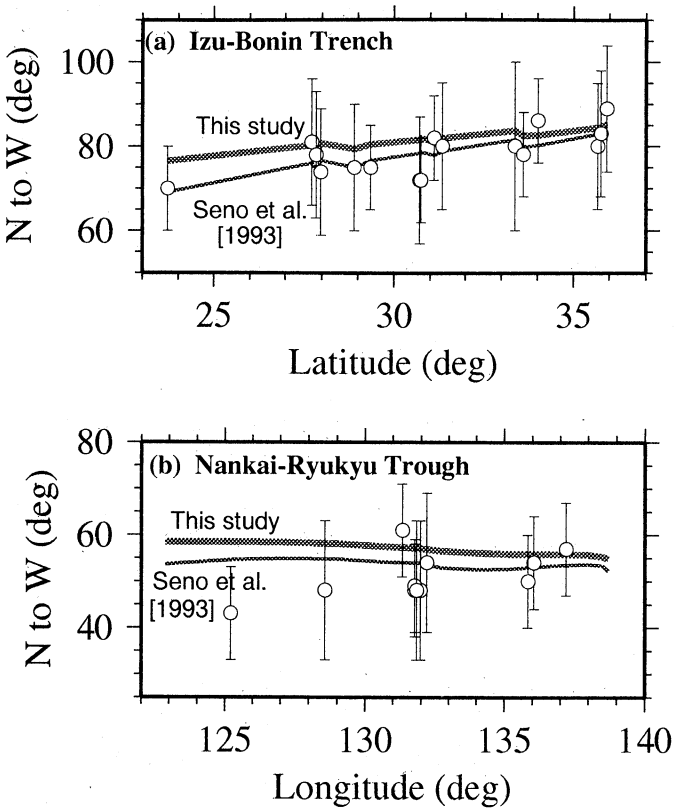

Figure 4. The predicted slip direction at (a) the Izu-Bonin Trench and (b) the Nankai Trough from the AM-PH Euler vectors determined by this study (thick line) and *Seno et al.* [1993] (thin line). Slip direction data and their 1σ uncertainties are after *Seno et al.* [1993].

5. Velocity Field of Southwest Japan: Decomposition Into Components

5.1. General Feature

In order to study deformation of an island arc using GPS velocity data, it is preferable to use velocities relative to the stable interior of the landward plate. For the moment we assume that the whole southwest Japan resides on AM, that is, we consider the Nankai Trough as the AM's southeastern boundary [*Wei and Seno*, 1998], rather than the Arima-Takatsuki Tectonic Line (ATTL) and the Median Tectonic Line (MTL) [*Ito et al.*, 1999] (Figure 1). Current activities of MTL will be discussed later on.

Figure 5 shows the velocity field of Southwest Japan relative to AM. Again, the velocity uncertainties are not drawn for the sake of visual simplicity (see section 3 for error evaluation). Velocity directions generally agree with the AM-PH convergence direction both in the Shikoku and Chugoku districts. As the velocity decreases monotonously toward the northwest, their azimuths change slightly but in a systematic manner: (1) azimuths at the southernmost sites, for example, those near the Muroto Cape deflect "counterclockwise" from the convergence direction, (2) those at about 150 km from the trough are undeflected, and (3) velocities deflect "clockwise" at sites farther to the northwest. We can see similar but somewhat different tendency in the Kinki district, where the first feature is significant at the southernmost Kii peninsula but the second and the third features are not evident. We will briefly discuss these features in the next section.

5.2. Elastic Response of the Arc Crust to Oblique Subduction

The direction of the AM-PH convergence in southwest Japan is not perpendicular to the strike of the Nankai Trough but deviates about 30° from it. Here we briefly discuss general characteristics of the crustal deformation in such a case. When the plate interface is partly locked, interseismic deformation in the island arc can be modeled by an imaginary backward slip at the locked fault surface (see *Savage* [1983] for a two-dimensional case). Since the slab dip angle is relatively low (7° ~ 15°) at the Nankai Trough, viscous flow in the asthenospheric wedge beneath the arc would not play an important role and an elastic half-space assumption would be reasonable for the interseismic timescale.

We begin with a simple three-dimensional model composed of a single rectangular fault 2000 km long and 170 km wide. It dips by 10° from its upper edge at the Earth's surface, so the lower edge is about 30 km deep. We give a unit back slip on the fault plane in the direction deviated by 30° counterclockwise from the downdip direction (Figure 6) and calculated the surface displacement following *Okada* [1992]. The result shown in Figure 6 demonstrates that displacement azimuths change systematically as a function of the distance from the trench. Counterclockwise deflection near the trough increases as we proceed inland from the trench. This becomes largest at about 150 km from the trench, which corresponds approximately to the surface projection of the lower edge of the fault. The counterclockwise deflection decreases as we go farther inland and becomes clockwise at about 175 km. In the most inland area the deviation increases and the velocity eventually becomes perpendicular to the trench. The displacement amplitude, on the other hand, decay monotonously as we go away from the trench, and the largest gradient is seen at about 150 km from the trench.

Savage [1983] pointed out that the crustal strain due to dip- and strike-slip movements at a thrust zone depend differently on the distance from the trench. The observed feature in southwest Japan could be understood by comparing the contributions from these two components of the dislocation. If the fault is sufficiently long, they will cause displacements normal to and parallel with the trough, respectively. In Figure 6 we plot the surface displacements in response to pure dip- and strike-slip fault displacement as functions of the distance from the trench. When the dip angle is 10°, displacement due to the strike-slip component is

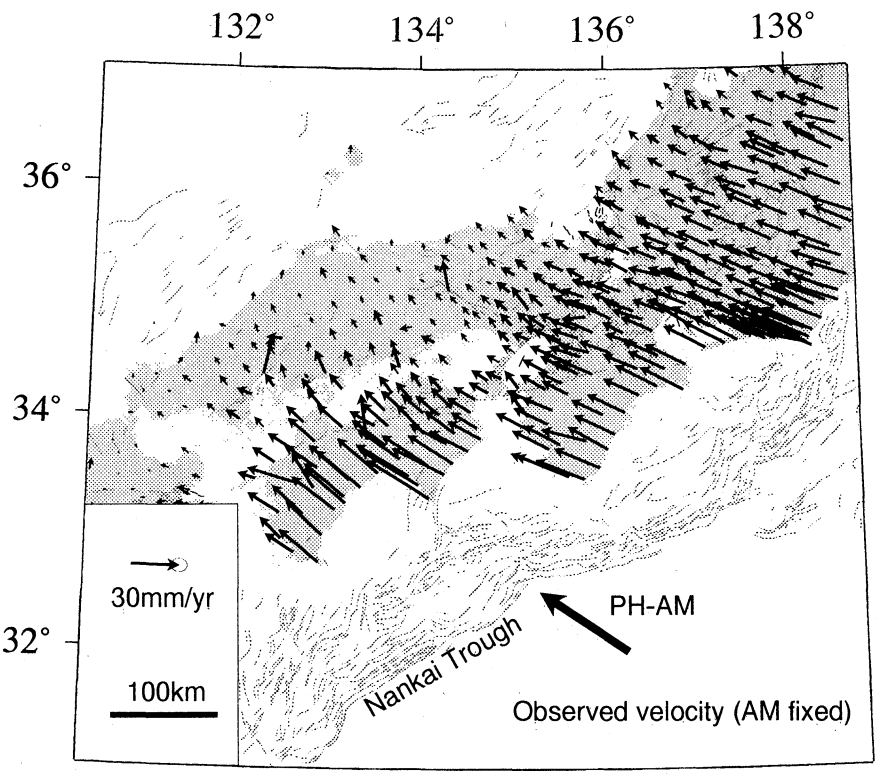

Figure 5. The interseismic crustal velocity field of southwest Japan with respect to the Amurian Plate. Velocity uncertainties are omitted for clarity (see Figure 2). The systematic eastward movement in the Chugoku district found in Figure 2 has disappeared. Instead, northwestward movements predominate throughout the Chugoku and Shikoku districts, reflecting the subduction of the Philippine Sea Plate at the Nankai Trough. In general, the azimuth of velocity vectors deviated clockwise to the north and counterclockwise in Kinki district to the northeast.

larger/smaller if the point is nearer/farther than 170 km from the trough. This difference in landward decays accounts for the changes in the surface displacement azimuths in Figure 6. We also found that a large dip angle (i.e., the deeper fault lower edges) causes a larger deflection. Velocities in Figure 6 resemble the observed ones in Figure 5, suggesting this simple fault model is a fine first-order approximation.

5.3. Inversion of Back Slip at the Nankai Trough

If the observed crustal deformation in southwest Japan (Figure 5) were due solely to the subduction at the Nankai Trough, we could estimate the back slip distribution at the surface of the PH slab by a conventional inversion approach. This has been done by, for example, *Ozawa et al.* [1999], *Ito et al.* [1999], and *Mazzotti et al.* [2000]. Because their velocity references were not ideal for such studies (see section 2.1), here we try a similar inversion using the AM-fixed velocity field.

We assume a homogeneous elastic half-space but a more realistic geometry for the plate interface faults than in section 5.2. The geometry of the upper surface of the PH slab is well determined from the distribution of microearthquakes [e.g., *Ishida*, 1992]. *Sagiya and Thatcher* [1999] assumed that the focal depths of such microearthquakes represent the upper surface of the PH slab and modeled the plate boundary as a smooth surface [see *Sagiya and Thatcher*, 1999, Figures 6]. To mimic the curved interface with multiple fault segments, they inverted terrestrial geodetic data using several competing models and obtained the optimal one composed of 32 segments [see *Sagiya and Thatcher*, 1999, Figure 6]. Because their fault model is optimized for terrestrial geodetic surveying data, the segments in shallower zones are made larger. The distribution of their data is similar to GEONET, and so we use their fault model as they are (however, we added a few more segments as far to the east as the off-Tokai district keeping their strategy for the fault segment sizes; Figure 7).

There are gaps and overlaps between the rectangular fault segments (Figure 7). We evaluated how much they affect the results by forward calculations as described in section 5.4 by extending and reducing the fault lengths by up to 20 km. We found that the velocity changes are normally less than 1 mm/yr and reaches about 2-3 mm/yr only at the sites closest to the trough. We also evaluated the effect of ignoring the southwestern extension of the fault in the same way. To represent

the most critical case, we extended our fault model to southwest and assumed full coupling at its shallower part and found that the change in velocities was only about 2-3 mm/yr at the southernmost sites in the studied area. Moreover, past studies suggested that this extended area is very weakly coupled [e.g., *Ozawa et al.*, 1999; *Ito et al.*, 1999], and so the cutoff effect would be much smaller than about 2-3 mm/yr even at the westernmost sites.

Most geodetic data are obtained in a land area or on one side of the plate boundary in Japan, which degrades the resolution of the back slip inversion to a large extent. To stabilize the solution, *Ozawa et al.* [1999] made fault segments much larger than ours. Here we take another approach, to impose a priori constraints to suppress excessive roughness of the fault slip distribution. We follow the ideas of *Jackson* [1979] and *Jackson and Matsu'ura* [1985] as summarized in the Appendix.

Strength of the plate coupling at the Nankai Trough has been inferred from a thermal model by *Hyndman et al.* [1995]. They inferred that the fully locked zone extends to the 25 km depth and the coupling linearly decreases with depth in the transitional zone at depth 25-35 km. The thermal model postulates viscous flows at depth and is not conceptually consistent with the elastic half-space assumed by us. However, we do not think viscous flow an important factor in the studied area because of the shallow dip angle of the slab (see section 5.2) and low stress level in the plate convergence direction (see section 2.2). *Mazzotti et al.* [2000] estimated the coupling ratio at the Nankai Trough using the GPS site velocities assuming an elastic half-space and found their results consistent with this thermal model. Although their velocity reference is not an ideal one, it suggests that the combination of the coupling predicted by the thermal model and the elastic half-space assumption is basically correct. They also found that the lower edge of the fully coupled zone is slightly better represented by an isodepth model than an isotherm model.

In this study we assumed full coupling for the fault segments with depths of 5-25 km, 50% for those in 25-35 km, 75% for those in 25-30 km, and 25% for those in the 30-35 km depth range. Back slip vectors are expected to align with the AM-PH convergence direction. We multiplied the plate convergence rate at the center of fault

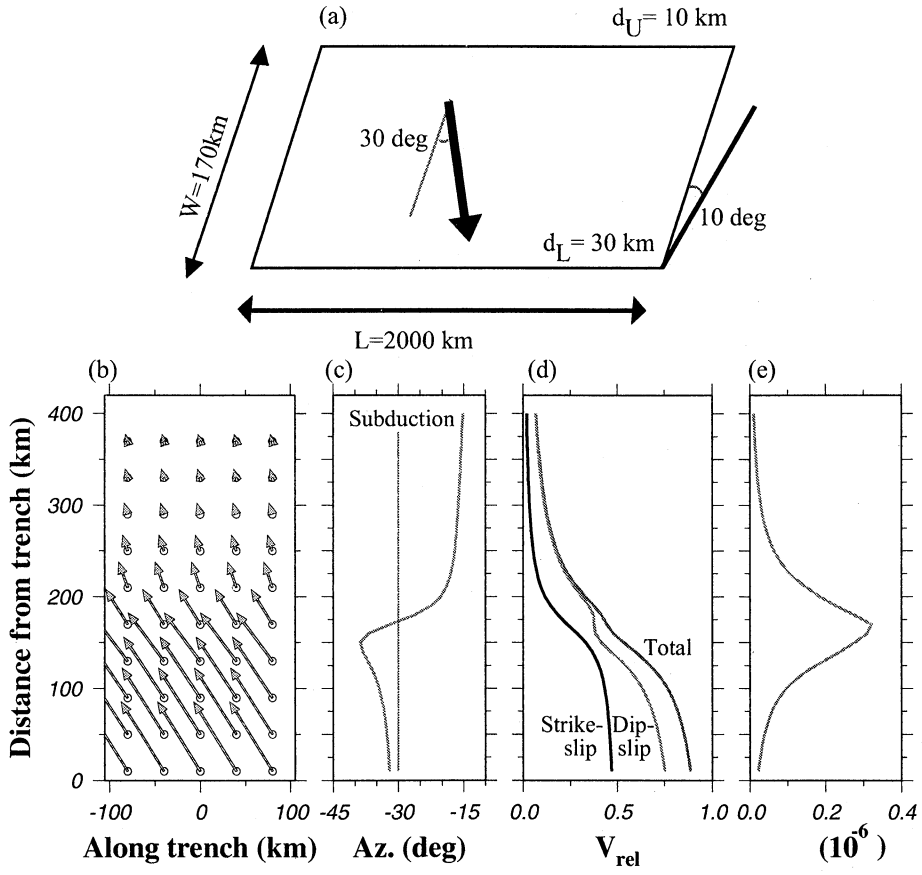

Figure 6. (a) Fault configuration of the simplified model of the Nankai Trough and predicted velocity field for unit back slip on this simple rectangular fault plate. (b) The spatial distribution of the calculated crustal velocity field. (c) The azimuths measured clockwise from trench normal. (d) The lengths of velocity vectors with respect to the distance from the trough. (e) The maximum shear strain rate.

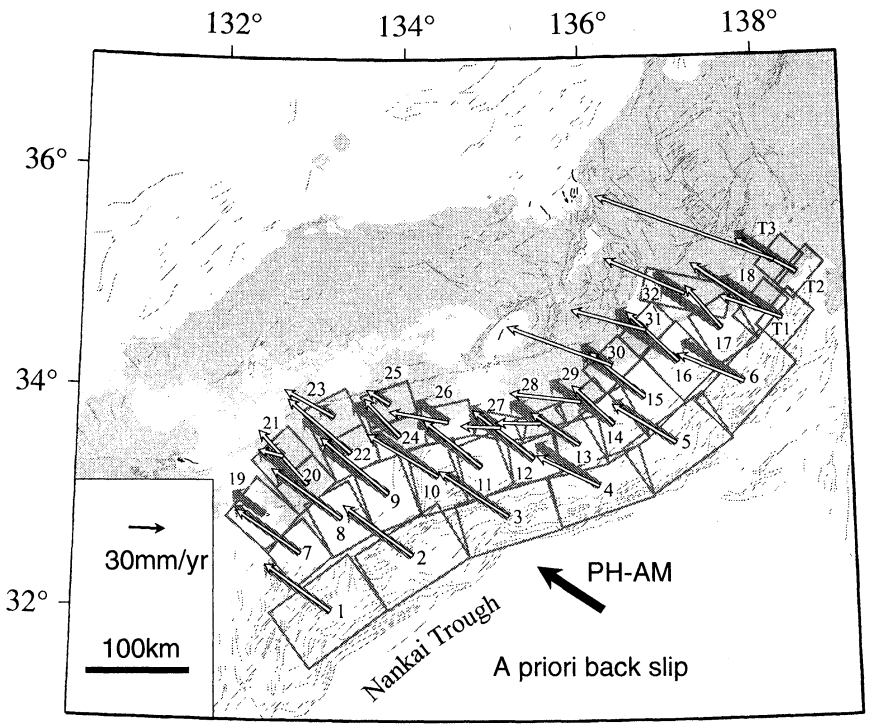

Figure 7. Fault geometry of the plate interface at the Nankai Trough and a priori back slip rate at each segment (thick gray arrows) and the estimated back slip rates by an inversion study (narrow open arrows). Original fault geometry was constructed by *Sagiya and Thatcher* [1999]. Three segments are added in Tokai district in the present study. The a priori back slips on the fault segments are parallel to the PH-AM convergence direction predicted by the Euler vector obtained in the present study, and their lengths are calculated using the coupling strengths from the thermal model of *Hyndman et al.* [1995]. Formal errors are, for most of the segments, about 15 mm/yr for both of strike and dip components. The partial resolution of data tend to be small for the shallower segments (mostly less than 30% for segments 1-6, 40-70% for 7-17 and T3, and greater than 80% for the rest.

segment by these factors and made them the a priori values of the back slip vectors (Figure 7). Among the fault segments, those in the transition zone were constrained 3 times as loosely as those for the rest considering larger ambiguity of the slip distribution there. For simplicity, we assumed that the a priori values of the model parameters are not mutually correlated. The scaling factors for the covariance matrices of data and a priori information are optimized so as to minimize the Akaike's Bayesian information criterion (ABIC) [*Akaike*, 1980].

Sagiya and Thatcher [1999] demonstrated that the coseismic slip distributions associated with the 1944 and 1946 events were highly nonuniform. After the 1994 Sanriku-Haruka-Oki earthquake, significant afterslip was observed and the afterslip was suggested to be larger where coseismic slips were smaller [*Heki et al.*, 1997; *Nishimura et al.*, 2000]. Therefore the nonuniformity in the coseismic slips of the 1944 and 1946 events merely reflect differences in frictional properties, and the total slips as well as interseismic coupling would be more uniformly distributed. Hence we assign uniform a priori constraint for the fully coupled segments.

The weighted residual sum of squares for data and for the a priori information is 0.95 and 0.52, respectively, and the normalized root-mean-square (nrms) defined by (A35) is 1.026. The partial resolution for data, defined by (A25), represents the contribution of data to the estimation. For example, fault segments with small a priori uncertainties tend to have a small data resolution value (mostly less than 10% for segments $1 \sim 6$, 30-60% for those $7 \sim 18$). Those with larger uncertainties generally have values larger than 70%. The standard deviation for the estimated parameters are typically $\sim$ 8-15 mm/yr for the fully coupled seismogenic zones and about 15-25 mm/yr for the transition zones, both for the strike- and dip-slip components. The estimated back slips, surface velocities calculated using the estimated back slips, and residual (observed minus calculated) velocities are shown in Figure 7, Figure 8a, and Figure 8b, respectively. Generally speaking, the observed velocities in the Chugoku and Shikoku districts are reproduced fairly well, including the subtle changes in the velocity azimuths, and the estimated slips off the Shikoku island agree well with the convergence direction. The situation is somewhat different in the Kinki district; the residual velocities (Figure 8b) still show systematic patterns and the estimated back slips tend to deflect counterclockwise from the AM-PH conver-

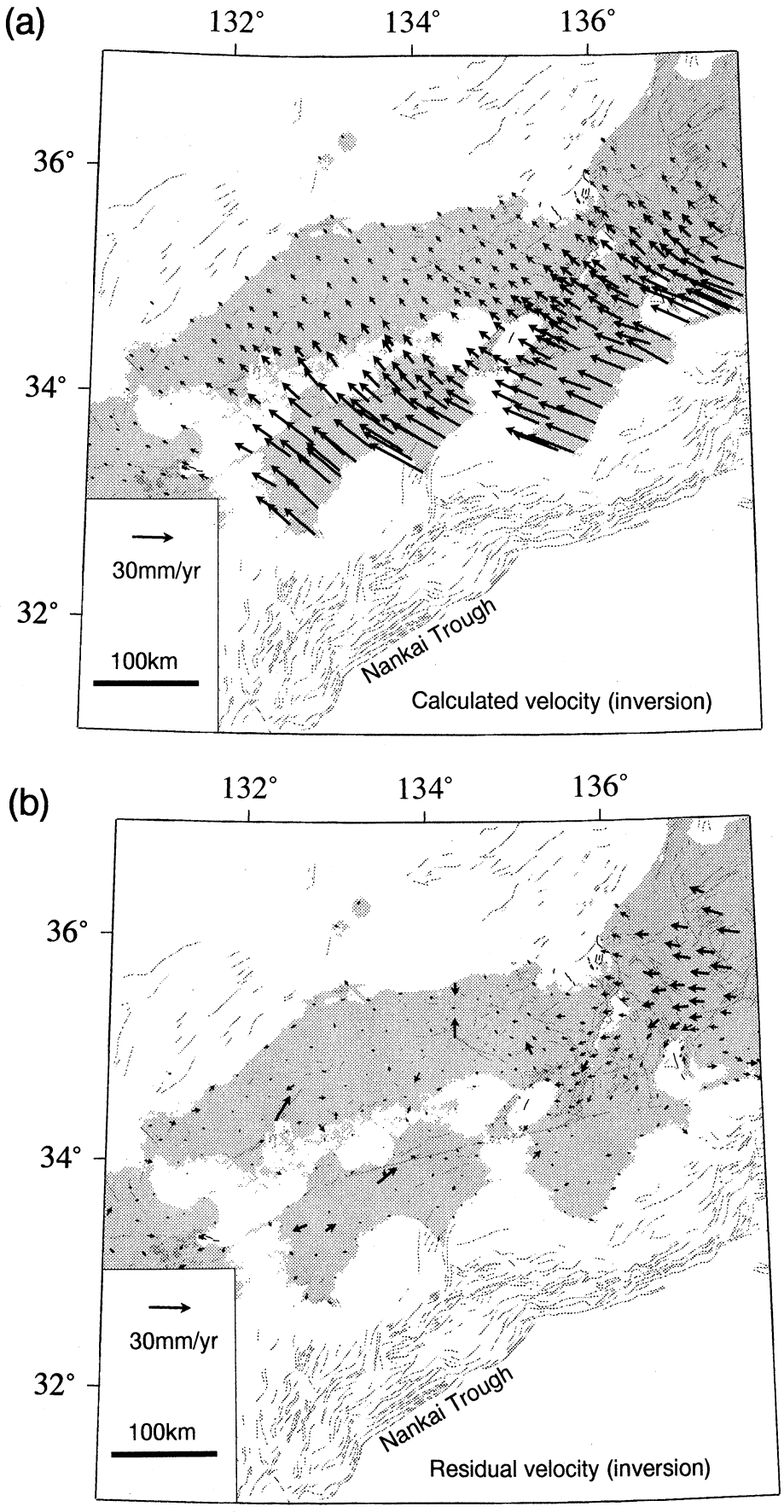

Figure 8. (a) The calculated velocity field from the back slip rates estimated by the inversion study. The basic characteristics of the observations (see Figure 6) are reproduced in the Chugoku and Shikoku districts. (b) The residual velocity field of the inversion study. A systematic westward velocity residual in Kinki district suggests that there is a deformation source other than the AM-PH convergence.

gence direction (Figure 7). These results suggest the limitation of attributing the entire crustal deformation in southwest Japan to the subduction.

Such a tendency is seen in the results of *Ozawa et al.* [1999], where residual velocities in the Kii Peninsula are smaller than ours, but the estimated backslip off the eastern part of the Kii Peninsula is much larger (89.0-115.2 mm/yr) than the AM-PH convergence and deflects counterclockwise from it by about 15-30°. These inversion results are possibly artifacts caused by attributing the crustal deformation only to subduction neglecting the crustal deformation due to the collision between the island arcs. These two components are not mutually orthogonal and difficult to discriminate by such an inversion approach. Strongly constraining the back slip direction to the plate convergence direction would help to some extent, but the nonorthogonality will still affect the estimated lengths of the back slip vectors. After all, we will need an alternative approach to isolate the nonsubduction origin crustal deformation.

5.4. Forward Calculation of the Subduction Effect and Extraction of the Collision Effect

In this section we perform a forward calculation to model crustal deformation due to the subduction at the Nankai Trough. We again employ the coupling strength inferred by the thermal model of *Hyndman et al.* [1995] and calculate the AM-PH relative movements using the Euler vector we obtained earlier in this study. The a priori back slip rates and the calculated velocities are shown in Figures 7 and 9a, respectively. By subtracting them from the observed velocities, we obtain the residual velocity field shown in Figure 9b, which would possibly show crustal deformation of collision origin.

The observed velocities in the Chugoku and Shikoku districts (Figure 5) are very consistent with those calculated (Figure 9a) both in direction and length, although no parameters are adjusted to bring them consistent with each other. This is also recognized in the smallness of the residual velocities in these districts in Figure 9b. In the Kinki district, on the other hand, residual velocities are large and systematic, suggesting the existence of crustal deformation caused by the collision between the continental lithospheres of southwest and northeast Japan. We use this velocity field for further geophysical discussions considering it better represents nonsubduction crustal deformation than the residual velocity field obtained by inversion in the previous section (Figure 8b).

6. Discussion

6.1. Interarc Collision in Japan

As mentioned earlier, E-W compressional stress fields prevail in southwest Japan. Because it is difficult to explain it by the elastic loading of the PA slab at the Japan Trench more than 500 km away, we have been assuming a plate boundary runs along the eastern margin of the Japan Sea down to ISTL, and the collision between the northeast and southwest Japan arc is responsible for this stress field. *Heki et al.* [1999] recently found that the convergence is between AM and NA and estimated the convergence rate in and around Japan to be about 16-18 mm/yr. Conventional ground geodetic surveys suggested that crustal shortening is accommodated by a broad zone to the west of ISTL [e.g., *Hashimoto and Jackson*, 1993]. This E-W compression is much stronger than the NW-SE compression due to the subduction and would cause significant crustal deformation especially in the Chubu and Kinki districts. In this section we discuss crustal deformation caused by this E-W compression.

The direction of the residual velocities in the Chubu district is consistent with the NA-AM convergence direction predicted by *Heki et al.* [1999] (Figure 9b). In the close-up view of the Kinki district (Figure 10), they seem to decay sharply and become mixed with the southward components in the southerly GPS sites. The consequences of the interarc collision in Japan can be compared to the Indo-Eurasian collision case. There crustal underthrusting and thickening occur in a relatively narrow zone in the Himalaya region as the direct consequence of the northward movement of the Indian subcontinent. As the secondary consequence, crustal blocks in an extensive region in eastern Asia are extruded eastward [*Molnar and Tapponnier*, 1975]. The east-west imbalance of the extrusion (i.e., no westward extrusion) comes from the existence of subduction zones in the eastern side of Eurasia. Such zones mechanically behave as a "free boundary" for extruded crustal blocks. Series of left(right)-lateral strike-slip faults striking NE-SW (NW-SE) develop north of the collision zone, and displacements along these faults transfer the northward movement of India to the lateral extrusion of crustal blocks. Direct space geodetic measurements in eastern Asia by VLBI [*Heki et al.*, 1995; *Heki*, 1996; *Molnar and Gipson*, 1996] and GPS [*Kato et al.*, 1998b; *Larson et al.*, 1999; *Heki et al.*, 1999] support this view.

In the present case the Chugoku district is relatively free from deformation and could be compared to the Indian subcontinent. Conjugate strike-slip fault systems (right-lateral NE-SW trending faults and left-lateral NW-SE trending faults) develop in the Kinki and Chubu districts and accommodate east-west shortening and north-south extension. Thus this region may correspond to central Asia. It is mechanically asymmetric: the Japan Sea side is a "fixed" boundary within AM, while the Pacific side may act as a "free" one because the Nankai Trough is there. The extrusion therefore becomes southward just like it is eastward in Asia, giving rise to the gradual counterclockwise rotation of the residual velocity directions in the Chubu district as we proceed to the west. Strictly speaking, such a southward velocity component implies a slightly higher con-

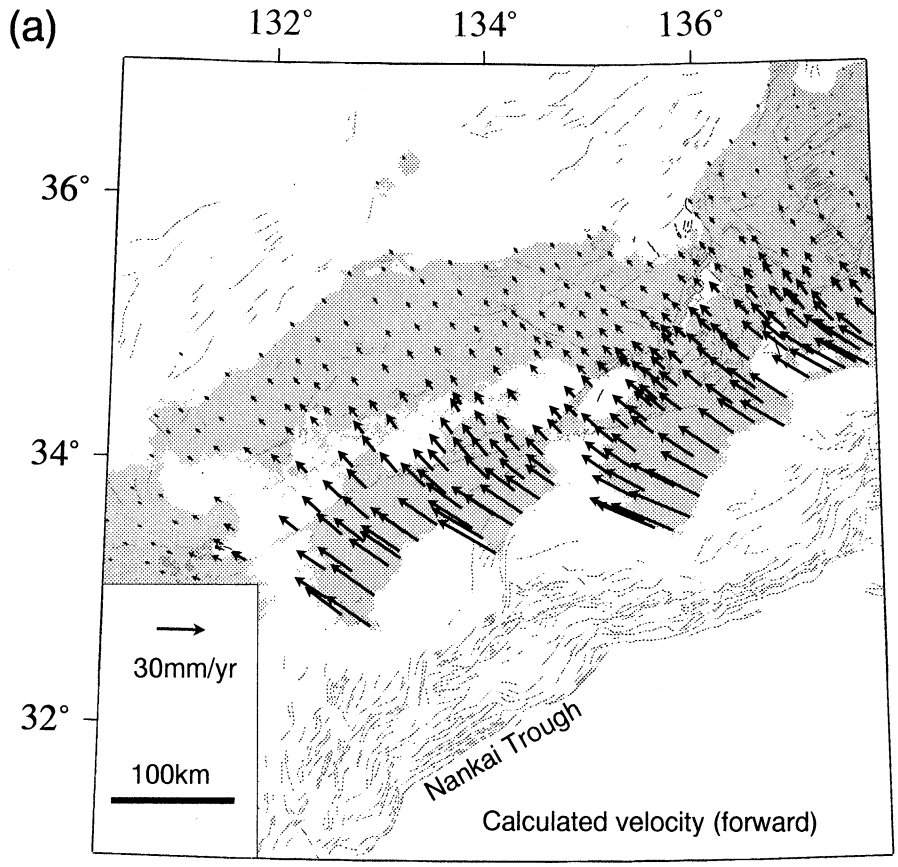
(a)
132°
134°
136°
36°
34°
32°
30mm/yr
100km
Nankai Trough
Calculated velocity (forward)

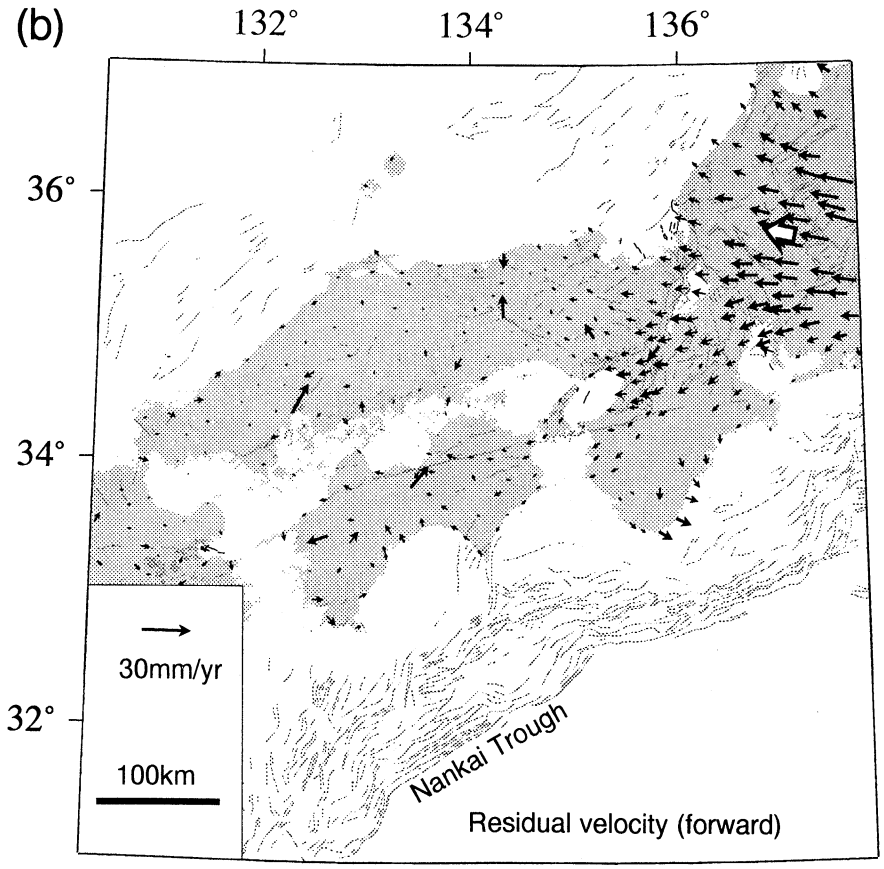
(b)
132°
134°
136°
36°
34°
32°
30mm/yr
100km
Nankai Trough
Residual velocity (forward)

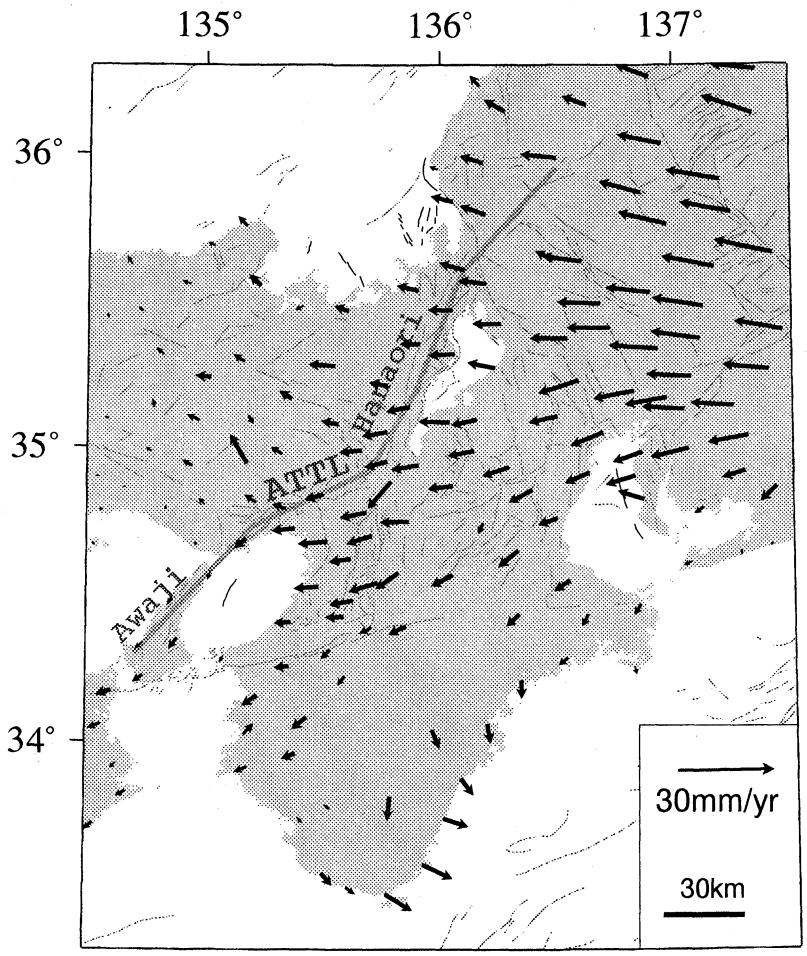

Figure 10. The residual velocity field of the forward calculation in Kinki district.

vergence rate in the trough to the south of Kinki than the plate tectonic prediction, and so the same coupling strength will cause more NW-SE contraction than depicted in Figure 7. We neglect this effect here because such a correction would be small enough.

The NW-SE shortening due to the elastic loading of the PH slab is cyclic by nature and controlled by the 100- to 200-year recurrence interval of interplate thrust earthquakes at the trough. This component would be elastic to a large extent, that is, the interseismic strains would be mostly released in the next interplate earthquake and not recorded as permanent crustal shortening. On the other hand, the E-W compression governs the crustal stress field and would accumulate over a geological timescale in the island arc crust through inland earthquakes in the brittle upper crust, and through ductile flows in the lower crust. *Thatcher* [1984] pointed out that the cumulative interseismic north-south shortening of southwest Japan is significantly smaller than coseismic north-south extension there, which may reflect long-term seaward movement of the leading edge of the island arc, that is, southward extrusion of the island arc lithosphere.

6.2. Fault Motion at the Median Tectonic Line

The Median Tectonic Line (MTL) is a vertical right-lateral strike-slip fault, running from the central Fossa Magna region, through the Kii peninsula, Shikoku

Figure 9. (a) The forward calculated velocity field based on the thermal model developed by *Hyndman et al.* [1995]. The basic features of the observed velocity field are well reproduced in Chugoku and Shikoku districts, including the systematic deflections of velocity field azimuths. (b) The residual velocity field of the forward calculation. This is characterized by a decrease in the westward movement of the GPS sites from east to west in the Kinki district and southward movement of the southerly sites in this district. The residual velocities in the Chubu district are generally in good agreement with the relative plate movement predicted by the AM-NA Euler vector (white arrow) obtained by *Heki et al.* [1999].

to Kyushu (Figure 1). Geological studies indicate an average displacement rate of about 5-10 mm/yr [*Okada*, 1973], and it is hence recognized as one of the most active inland faults in Japan. In spite of the high rate suggested by neotectonic studies, no large earthquakes have been known at MTL for more than 1000 years. Hence direct space geodetic observations of the current slip rate and the coupling depth are important in assessing the future seismic hazards in this region. However, since the rate 5-10 mm/yr is much smaller than the plate convergence rate at the Nankai Trough, it is easily masked by the interseismic elastic straining. It has therefore been uncertain whether MTL currently accommodates any strike-slip movements by creep. If the upper portion (shallower than 15 km) of MTL creeped like the central creeping section of the San Andreas Fault [*Burford and Harsh*, 1980; *Schulz et al.*, 1982], the velocity field would have a sharp discontinuity there. Even if the upper portion was locked, creep in its lower extension would still result in a gradual change of the velocity field across MTL [*Hashimoto and Jackson*, 1993].

Hashimoto and Jackson [1993] assumed MTL to be a tectonic boundary dividing southwest Japan into the inner and the outer zones. Using century-long geodetic data, they estimated the displacement rate at its downward extension to be 5 ± 3 mm/yr in a right-lateral sense. Later, *Sagiya* [1995] compiled triangulation, trilateration, leveling, and tide gage data in Shikoku and found that postseismic slip following the successive two earthquakes at the Nankai Trough (the Nankaido and Tonankai Earthquakes) continued around the main rupture region and its downdip extension for at least 20 years. Because the AM-PH plate convergence is not perpendicular to the MTL strike, it is likely that the data used by *Hashimoto and Jackson* [1993] were affected by such postseismic effects. Therefore we examine the MTL motion in a shorter time span using space geodetic data during an interseismic period.

In the velocity field shown in Figure 9b the deformation due to the elastic loading at the Nankai Trough is removed. At a first glance we see a velocity difference across MTL in Shikoku consistent with geological estimates, that is, the outer zone moves west-southwestward by 2-5 mm/yr while the inner zone is stationary with respect to AM. In Figure 11 we show crustal movements calculated assuming that MTL is vertical and its lower part is freely slipping by 5 mm/yr while its upper part (0-15 km in depth) is fully locked. The latter effect is calculated assuming an elastic half-space using the formula by *Okada* [1992]. The calculated velocity field could explain components parallel with MTL in the residual velocity field, although there still remain components in the subduction direction, suggesting that the subduction-origin crustal deformation is not completely corrected yet.

Next we evaluate the MTL motion in a different approach. If the a priori back slips given at the Nankai Trough were inaccurate (e.g., in the deeper transient zone), it might cause spurious residual velocities that could be misunderstood as the MTL motion. Here we estimate the coupling at the Nankai Trough and the MTL motion simultaneously from the observed velocity field. We employ the same inversion method as the previous section (Appendix) but used velocities only in the Chugoku and Shikoku districts to prevent crustal deformations of other tectonic origins (e.g., the arc-arc collision) from affecting the estimation of the fault slips at the Nankai Trough and MTL. We assume two blocks, that is, the inner and outer zones. Since the observed velocities are relative to AM, we fixed the motion of

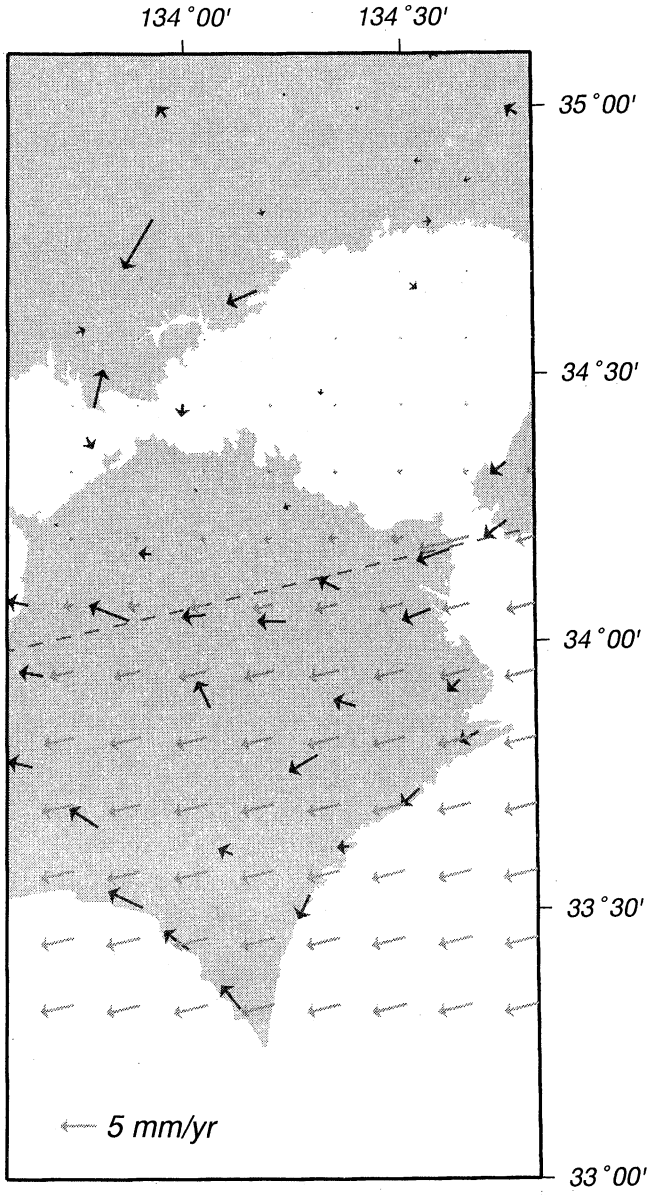

Figure 11. The residual field of the forward calculation (solid vector) and the calculated crustal deformation (shaded vectors) caused by the elastic loading of the Median Tectonic Line (MTL). We assumed that MTL is vertical and its lower extension is freely slipping at 5 mm/yr while its upper part (0-15 km in depth) is fully locked.

Table 2. Fault Parameters for the Median Tectonic Line[a]

Segment	Latitude, deg	Longitude, deg	D, km	W, km	L, km	ϕ, deg	δ, deg
M1	34.2	134.7	0	15	49	243	90
M2	34.1	134.2	0	15	45	252	90
M3	34.0	133.7	0	15	64	259	90
M4	33.9	133.0	0	15	62	259	90
M5	33.6	132.4	0	15	50	259	90

[a] D, depth of the upper edge; W, width; L, length; ϕ, strike measured clockwise from the north; δ, rake angle.

the inner zone to zero. Thus velocities in the inner zone are composed of only the contributions from the slip deficits at the Nankai Trough and MTL, while the block motion is added to them in the outer zone. We divide MTL into five vertical subfaults (Table 2), and we divide the Nankai Trough into 21 segments (segments 1-4, 7-13, 19-28 in Figure 7). As the a priori information, we assigned 5 mm/yr for the right-lateral direction and 0 mm/yr for the direction normal to it as the block velocity of the outer zone, back slip of 5 mm/yr at MTL, and the backslip at the Nankai Trough same as those in section 5.3. We impose uniform a priori constraints for all fault segments of the seismogenic zone at the Nankai Trough, and those 3 times as large for those of the transitional zone at the Nankai Trough, MTL segments, and the block velocity of the outer zone.

The inversion result is shown in Figure 12. The weighted residual sum of squares of data and of the a priori information is 0.93 and 0.32, respectively, and the nrms is 1.09. Although we do not see any systematic behaviors in the residual velocities, several outliers contribute much to the relatively high average of the residuals. On the other hand, residual of the a priori information is significantly smaller than the inversion for the Nankai Trough as shown in section 5.3. The partial resolution of data is smaller than 5% for segments 1 $\sim$ 4, 12 $\sim$ 13, and 28 at the Nankai Trough, 10-20% for 7 $\sim$ 11 and 27, 50-70% for 19 $\sim$ 26, but as large as 90% for all MTL segments except for segment M5 (55%) and larger than 99% for the block velocity. The standard deviation of estimated back slip rates are about 5 mm/yr for 1 $\sim$ 13, about 10 mm/yr for 19 $\sim$ 28 and M5, and 4-6 mm/yr for M1 $\sim$ M4. Statistical results suggested that the contribution of the back slip at MTL is not significant (i.e., the estimated values do not exceed their formal uncertainties) although the

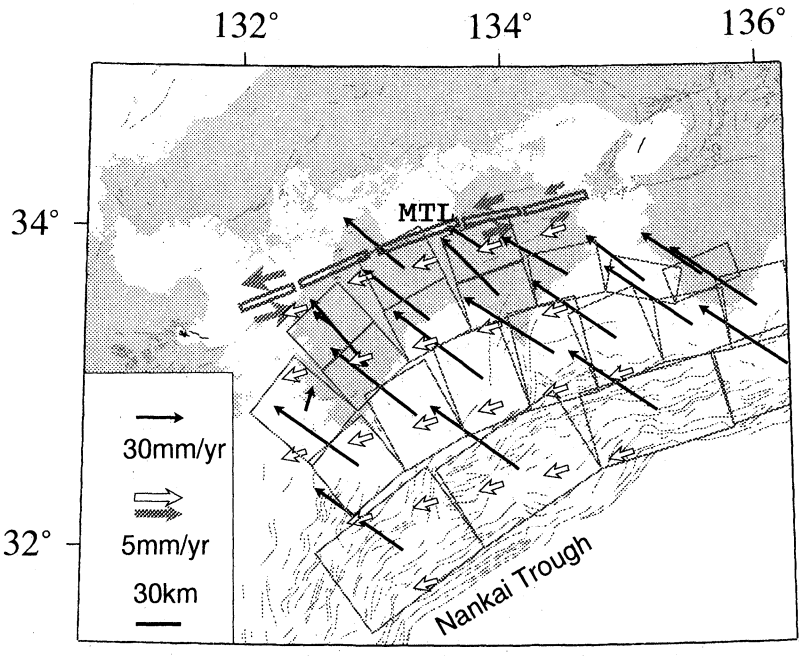

Figure 12. Estimated back slip rates at the Nankai Trough and the Median Tectonic Line (MTL), and the block movement of the outer zone with respect to the Amurian Plate. Note that the scale for back slip rate at the Nankai Trough is different from the others. The formal uncertainties for back slip rates at the Nankai Trough are typically 5-15 mm/yr. The estimated back slip rates at the MTL did not exceed their formal uncertainties. On the other hand, the block velocity of the outer zone is significant.

block movement itself was significant (-2.5 ± 1.1 mm/yr for the east and -0.8 ± 0.7 mm/yr for the north). In other words, the current GPS data require MTL to be a block boundary but does not require it to be locked at depth.

These results suggest that MTL is a tectonic boundary that divides Chugoku and Shikoku districts into the inner and the outer zones. It accommodates right-lateral movements of about 2-3 mm/yr; the inner zone is a part of AM while the outer zone moves toward the west-southwest as a forearc sliver. However, we could not draw significant information on the locking depth of MTL in spite of the current high density of permanent GPS points in Japan. Campaign observations with a denser GPS network across MTL in the eastern Shikoku district started in 1998 [*Tabei et al.*, 1999], and their future results would better constrain the kinematics of MTL.

This result is relevant to the question whether current crustal movements in Japan are better described by a block fault system [e.g., *Matsu'ura et al.*, 1986; *Hashimoto and Jackson*, 1993] or by a deformation of a continuum [e.g., *England and McKenzie*, 1982; *Houseman and England*, 1993]. Clear velocity contrasts in the residual velocity field across several active faults as well as MTL (Figure 10) may favor the former, but gradual velocity changes in more easterly areas may favor the latter. Since the collision effect does not extend to the Chugoku district (Figure 9b), these faults would be the western limit of the broad zone of collisional deformation (its eastern limit is ISTL; see section 2). If crustal movements are governed by ductile flow at depth, then the active faults might be only playing their passive role, that is, they move occasionally to release tectonic stress in the upper brittle part caused by the ductile flow underneath.

7. Conclusion

The interseismic velocity field in southwest Japan observed by the nationwide permanent GPS array over a 3-year period was investigated. The velocities were first converted to those with respect to the Amurian Plate to visualize intraplate crustal deformation. The azimuths of the observed velocities changed systematically across the arc, which was explained as a general feature of oblique subduction. Second, we estimated the back slip distribution at the Nankai Trough by a conventional inversion approach but found that the estimated back slip vectors deviate counterclockwise from the convergence directions in the eastern part of the studied area. This made us suspect the validity of the inversion approach. There seems to exist another source of crustal deformation to which little attention has been made so far. We attributed it to the collision of southwest Japan with northeast Japan, an inevitable consequence of the eastward movement of the Amurian Plate.

We modeled the elastic straining due to the subduction by a forward calculation incorporating thermal constraints of the plate interface and the newly obtained Euler vector between the Amurian and the Philippine Sea Plates. The calculated velocities, although no parameters were adjusted, agreed well with the observed velocities in the Chugoku and Shikoku districts. Residual velocities were systematic within and to the east of the Kinki district and were characterized by east-west contraction due to the convergence of the island arcs. This contraction seemed to be accommodated by the north-south extension rather than the crustal uplift as indicated by the dominance of strike-slip faults in central Japan. This extension causes the southward extrusion of the crust in the Kinki district, analogous to the eastward extrusion of crustal blocks in Asia due to the Indo-Eurasian collision. We found crustal velocity contrast across the Median Tectonic Line (MTL) in Shikoku. Our inversion study showed that MTL accommodates a right-lateral movement of about 2-3 mm/yr. The MTL, together with the faults running along the western coast of the Awaji island, the Arima-Takatsuki Tectonic Line (ATTL) and the Hanaori fault, may constitute the western limit of the interarc collision zone.

In order to discriminate the crustal deformation by subduction and collision, we preferred a simple forward calculation approach to sophisticated mathematical techniques. Nevertheless, we could clarify the basic features of the complicated crustal deformation pattern in southwest Japan. The key factors in this study include the adoption of the kinematic reference frame fixed to the Amurian Plate, usage of the a priori back slip vectors derived from the newly estimated Euler vector between the Amurian and the Philippine Sea Plates, and the coupling strength predicted by a thermal model. Clear understanding of crustal dynamics in southwest Japan will help us investigate if there is a causal relationship between the occurrence of inland earthquakes, for example, the 1995 Kobe earthquake, and interplate thrust earthquakes at the Nankai Trough. *Mogi* [1969] found that the activity of the inland earthquakes in southwest Japan increases toward the end of the cycles of the interplate thrust earthquakes at the Nankai Trough. Recently, *Hori and Oike* [1999] confirmed that inland earthquake activity remains significantly high for several decades before and up to a decade after great interplate earthquakes. Crustal deformation observations with high temporal and spatial density will provide a clue to understand fully the complicated seismotectonics in southwest Japan and to identify the existence of a trigger mechanism between these earthquakes.

Appendix A: Use of A Priori Information in a Linear Inversion

Let us assume that the unknown model parameter vector of M components to be $\mathbf{m}$, and the data vector of N components to be $\mathbf{d}$. Observation equation is

$$\mathbf{d} = G\mathbf{m} + \mathbf{e}, \tag{A1}$$

where G is a $N \times M$ data kernel and $\mathbf{e}$ is an observation error vector. For simplicity we assume the error $\mathbf{e}$ to be Gaussian with zero mean and covariance $\sigma^2\Sigma_d$:

$$\mathbf{e} \sim N(0, \sigma^2\Sigma_d), \tag{A2}$$

where σ^2 is an unknown scale factor for the covariance of $\mathbf{e}$. From (A1) and (A2) we have a stochastic model which relates the data $\mathbf{d}$ with the model parameter $\mathbf{m}$ as

$$\begin{aligned} p(\mathbf{d}|\mathbf{m};\sigma^2) &= (2\pi\sigma^2)^{-N/2}|\Sigma_d|^{-1/2} \\ &\quad \cdot \exp[-\frac{1}{2\sigma^2}(\mathbf{d} - G\mathbf{m})^T\Sigma_d^{-1}(\mathbf{d} - G\mathbf{m})], \end{aligned} \tag{A3}$$

where $|\Sigma_d|$ is the absolute value of the determinant of Σ_d. A priori information is also expressed by an observation equation [*Jackson*, 1979]. Assuming the a priori information vector of M components to be $\mathbf{p}$, the observation equation for a priori information becomes

$$\mathbf{p} = \mathbf{m} + \delta. \tag{A4}$$

We assume the error δ to be also Gaussian with zero mean and covariance $\alpha^2\Sigma_m$:

$$\delta \sim N(0, \alpha^2\Sigma_m), \tag{A5}$$

where α^2 is an unknown scale factor for the covariance of δ. Equations (A4) and (A5) allow us to have a stochastic model which relates the a priori information $\mathbf{p}$ with the model parameter $\mathbf{m}$ as

$$\begin{aligned} p(\mathbf{m};\alpha^2) &= (2\pi\alpha^2)^{-M/2}|\Sigma_m|^{-1/2} \\ &\quad \cdot \exp[-\frac{1}{2\alpha^2}(\mathbf{p} - \mathbf{m})^T\Sigma_m^{-1}(\mathbf{p} - \mathbf{m})]. \end{aligned} \tag{A6}$$

We can incorporate the probability distribution of the a priori information (A6) with that of the data (A3) using Bayes' theorem [*Jackson and Matsu'ura*, 1985] as

$$\begin{aligned} p(\mathbf{m};\sigma^2,\alpha^2|\mathbf{d}) &= cp(\mathbf{d}|\mathbf{m};\sigma^2)p(\mathbf{m};\alpha^2) \\ &= c(2\pi\sigma^2)^{-N/2}(2\pi\alpha^2)^{-M/2} \\ &\quad \cdot|\Sigma_d|^{-1/2}|\Sigma_m|^{-1/2}\exp[-\frac{1}{2\sigma^2}s(\mathbf{m})], \end{aligned} \tag{A7}$$

where

$$\begin{aligned} s(\mathbf{m}) &= (\mathbf{d} - G\mathbf{m})^T\Sigma_d^{-1}(\mathbf{d} - G\mathbf{m}) \\ &\quad +\beta^2(\mathbf{p} - \mathbf{m})^T\Sigma_m^{-1}(\mathbf{p} - \mathbf{m}), \end{aligned} \tag{A8}$$

$$\beta^2 = \frac{\sigma^2}{\alpha^2}. \tag{A9}$$

The maximum likelihood is realized when $s(\mathbf{m})$ is minimized. The necessary condition for this leads the basic equation

$$G^T\Sigma_d^{-1}(\mathbf{d} - G\mathbf{m}) + \beta^2\Sigma_m^{-1}(\mathbf{p} - \mathbf{m}) = 0. \tag{A10}$$

The solution and covariance matrix are given by

$$\mathbf{m}_{\rm est} = (G^T\Sigma_d^{-1}G + \beta^2\Sigma_m^{-1})^{-1}(G^T\Sigma_d^{-1}\mathbf{d} + \beta^2\Sigma_m^{-1}\mathbf{p}), \tag{A11}$$

$$C_m = \sigma^2(G^T\Sigma_d^{-1}G + \beta^2\Sigma_m^{-1})^{-1}. \tag{A12}$$

Unknown hyperparameters σ^2 and β^2 are estimated by minimizing a Bayesian information criterion (ABIC) proposed by *Akaike* [1980]. In the present case the number of adjustable hyperparameters is definite, and therefore ABIC is defined by

$$\mathrm{ABIC} = -2\log L(\sigma^2,\beta^2), \tag{A13}$$

where L is the so-called marginal likelihood of hyperparameters σ^2 and β^2:

$$\begin{aligned} L(\sigma^2,\beta^2) &= \int p(\mathbf{d}|\mathbf{m};\sigma^2)p(\mathbf{m};\alpha^2)d\mathbf{m} \\ &= (2\pi\sigma^2)^{-N/2}(\beta^2)^{M/2}|\Sigma_d|^{-1/2}|\Sigma_m|^{-1/2} \\ &\quad \cdot|G^T\Sigma_d^{-1}G + \beta^2\Sigma_m^{-1}|^{-1/2} \\ &\quad \cdot\exp[-\frac{1}{2\sigma^2}s(\mathbf{m}_{\rm est})]. \end{aligned} \tag{A14}$$

ABIC is minimized when $L(\sigma^2,\beta^2)$ is maximized. Thus

$$\frac{\partial L(\sigma^2,\beta^2)}{\partial\sigma^2} = \frac{\partial L(\sigma^2,\beta^2)}{\partial\beta^2} = 0 \tag{A15}$$

which leads

$$\sigma^2 = \frac{s(\mathbf{m}_{\rm est})}{N}. \tag{A16}$$

Substituting (A16) into (A14), we obtain

$$\begin{aligned} \mathrm{ABIC}(\beta^2) &= N\log s(\mathbf{m}_{\rm est}) - M\log\beta^2 \\ &\quad +\log|G^T\Sigma_d^{-1}G + \beta^2\Sigma_m^{-1}| \\ &\quad +N\left(\log\frac{2\pi}{N}\right) + \log|\Sigma_d| + \log|\Sigma_m|. \end{aligned} \tag{A17}$$

Let us denote the β^2 estimate that minimizes ABIC(β^2) as $\hat{\beta}^2$, then

$$\begin{aligned} \hat{\sigma}^2 &= \frac{s(\hat{\mathbf{m}}_{\rm est})}{N} \\ \hat{\alpha}^2 &= \frac{\hat{\sigma}^2}{\hat{\beta}^2} \end{aligned} \tag{A18}$$

$$\hat{\mathbf{m}}_{\rm est} = (G^T\Sigma_d^{-1}G + \hat{\beta}^2\Sigma_m^{-1})^{-1}(G^T\Sigma_d^{-1}\mathbf{d} + \hat{\beta}^2\Sigma_m^{-1}\mathbf{p}), \tag{A19}$$

$$\hat{C}_m = \hat{\sigma}^2(G^T\Sigma_d^{-1}G + \hat{\beta}^2\Sigma_m^{-1})^{-1}. \tag{A20}$$

The partial resolution matrices are derived by substituting (A1) and (A4) into (A11) and solving it with $\mathbf{m}_{\rm est}$:

$$\mathbf{m}_{\rm est} = HG\mathbf{m} + K\mathbf{m} + H\mathbf{e} + K\delta, \tag{A21}$$

where

$$H = (G^T\Sigma_d^{-1}G + \hat{\beta}^2\Sigma_m^{-1})^{-1}G^T\Sigma_d^{-1}, \quad \text{(A22)}$$

$$K = (G^T\Sigma_d^{-1}G + \hat{\beta}^2\Sigma_m^{-1})^{-1}\hat{\beta}^2\Sigma_m^{-1}. \quad \text{(A23)}$$

By taking the stochastic average, we obtain

$$< \mathbf{m}_{\rm est} >= R^{\rm obs}\mathbf{m} + R^{\rm apr}\mathbf{m}, \quad \text{(A24)}$$

where

$$R^{\rm obs} = HG \quad \text{(A25)}$$

$$R^{\rm apr} = K \quad \text{(A26)}$$

are the partial resolution matrices for the data and the a priori information, respectively. Finally, we can calculate the predicted values of $\mathbf{d}$ from $\hat{\mathbf{m}}_{\rm est}$ as

$$\hat{\mathbf{d}}_{\rm est} = G\hat{\mathbf{m}}_{\rm est} \quad \text{(A27)}$$

$$\hat{C}_d = G\hat{C}_m G^T. \quad \text{(A28)}$$

The misfit is measured by the weighted residual sum of squares

$$\frac{1}{\hat{\sigma}^2}\frac{(\mathbf{d} - G\hat{\mathbf{m}}_{\rm est})^T\Sigma_d^{-1}(\mathbf{d} - G\hat{\mathbf{m}}_{\rm est})}{N}, \quad \text{(A29)}$$

for data and

$$\frac{1}{\hat{\alpha}^2}\frac{(\mathbf{p} - \hat{\mathbf{m}}_{\rm est})^T\Sigma_m^{-1}(\mathbf{p} - \hat{\mathbf{m}}_{\rm est})}{M} \quad \text{(A30)}$$

for the a priori information, respectively. Variable χ^2 is defined as

$$\chi^2 = \frac{1}{\sigma^2}(\mathbf{d} - G\mathbf{m})^T\Sigma_d^{-1}(\mathbf{d} - G\mathbf{m}) + \frac{1}{\alpha^2}(\mathbf{p} - \mathbf{m})^T\Sigma_m^{-1}(\mathbf{p} - \mathbf{m}). \quad \text{(A31)}$$

For the optimized solution $\hat{\mathbf{m}}_{\rm est}$,

$$\begin{aligned}\chi^2 &= \frac{1}{\hat{\sigma}^2}(\mathbf{d} - G\hat{\mathbf{m}}_{\rm est})^T\Sigma_d^{-1}(\mathbf{d} - G\hat{\mathbf{m}}_{\rm est}) \\ &\quad + \frac{1}{\hat{\alpha}^2}(\mathbf{p} - \hat{\mathbf{m}}_{\rm est})^T\Sigma_m^{-1}(\mathbf{p} - \hat{\mathbf{m}}_{\rm est}) \\ &= \frac{1}{\sigma^2}s(\hat{\mathbf{m}}_{\rm est}) \\ &= N. \end{aligned} \quad \text{(A32)}$$

The degree of freedom for this type of inversion is given by *Dong et al.* [1998] as

$$N - M + N_c \quad \text{(A33)}$$

where

$$N_c = tr((R^{\rm obs})^{-1}). \quad \text{(A34)}$$

N_c represents the effective estimated parameter dimension under general constraints and satisfies

$N_c \to M$ when $\Sigma_m \to \inf$,
$N_c \to M - k$ when $\Sigma_m \to 0$,
$M - k \le N_c \le M$,

where k is the number of a priori information. In this case the degree of freedom is in general no longer an integer. Finally, the normalized root-mean-square (nrms) is defined as

$$\text{nrms} = \sqrt{\frac{\chi^2}{N - M + N_c}}. \quad \text{(A35)}$$

See *Dong et al.* [1998] for the detail.

Acknowledgments. We thank Paul Segall, Mark Murray (Stanford University), Danan Dong (JPL) for their valuable comments, suggestions, and discussions, and we thank Kelin Wang (Geological Survey of Canada) for sending his preprints. Critical reviews by Timothy Dixon, Steven Cohen, and Robert McCaffrey improved the quality of the paper. Part of this study was done during S.M.'s stay at Stanford University, supported by The Long-Term Scholarship Program of the Science and Technology Agency, Government of Japan. A software package, Generic Mapping Tool (GMT), was used to plot the figures.

References

Akaike, H., Likelihood and the Bayes procedure, in *Bayesian Statistics*, edited by J.M. Bernardo, M.H. DeGroot, D.V. Lindly, and A.F.M. Smith, pp. 143-166, University, Valencia, Spain, 1980.

Ando, M., Source mechanisms and tectonic significance of historical earthquakes along the Nankai Trough, Japan, *Tectonophysics, 27,* 119-140, 1975.

Argus, D.F., and R.G. Gordon, No-net-rotation model of current plate velocities incorporating plate motion model NUVEL-1, *Geophys. Res. Lett., 18,* 2039-2042, 1991.

Burford, R.O., and P.W. Harsh, Slip on the San Andreas fault in central California from a linement array surveys, *Bull. Seismol. Soc. Am., 70,* 1233-1261, 1980.

DeMets, C., R.G. Gordon, D.F. Argus, and S. Stein, Effect of recent revisions to the geomagnetic reversal time scale on estimates of current plate motions, *Geophys. Res. Lett., 21,* 2191-2194, 1994.

Dixon, T.H., M. Miller, F. Farina, H. Wang, and D. Johnson, Present-day motion of the Sierra Nevada block and some tectonic implications for the Basin and Range province, North American Cordillera, *Tectonics, 19,* 1-24, 2000.

Dong, D., T.A. Herring, and R.W. King, Estimating regional deformation from a combination of space and terrestrial geodetic data, *J. Geod., 72,* 200-214, 1998.

England, P., and D.P. McKenzie, A thin viscous sheet model for continental deformation, *Geophys. J. R. Astron. Soc., 70,* 295-321, 1982.

Hashimoto, M., Horizontal strain rates in the Japanese islands during interseismic period deduced from geodetic surveys, *Zisin, 43,* 13-26, 1990.

Hashimoto, M., and D.D. Jackson, Plate tectonics and crustal deformation around the Japanese Islands, *J. Geophys. Res., 98,* 16,149-16,166, 1993.

Hashimoto, M., T. Sagiya, H. Tsuji, Y. Hatanaka, and T. Tada, Co-seismic displacements of the 1995 Hyogo-ken Nanbu earthquake, *J. Phys. Earth, 44,* 225-279, 1996.

Heki, K., Horizontal and vertical crustal movements from three-dimensional very long baseline interferometry kinematic reference frame: Implication for the reversal timescale revision, *J. Geophys. Res., 101,* 3187-3198, 1996.

Heki, K., et al., Movement of the Shanghai station: Implication for the tectonics of Eastern Asia, *J. Comm. Res. Lab., 42,* 65-72, 1995.

Heki, K., S. Miyazaki, and H. Tsuji, Silent fault slip following an interplate earthquake at the Japan Trench, *Nature, 386,* 595-598, 1997.

Heki, K., S. Miyazaki, H. Takahashi, M. Kasahara, F. Kimata, S. Miura, N.F. Vasilenko, A. Ivashchenko, and K. An, The Amurian plate motion and current plate kinematics in eastern Asia, *J. Geophys. Res., 104,* 29,147-29,155, 1999.

Hirose, H., K. Hirahara, F. Kimata, N. Fujii, and S. Miyazaki, A slow thrust slip event following the two 1996 Hyuganada earthquakes beneath the Bungo Channel, southwest Japan, *Geophys. Res. Lett., 26,* 3237-3240, 1999.

Hori, T., and K. Oike, A physical mechanism for temporal variation in Southwest Japan related to the great interplate earthquake along the Nankai Trough, *Tectonophysics, 308,* 83-98, 1999.

Houseman, G., and P. England, Crustal thickening versus lateral expulsion in the Indian-Asian continental collision, *J. Geophys. Res., 98,* 12,233-12,249, 1993.

Huzita, K., Role of the Median Tectonic Line in the Quaternary tectonics of the Japan islands, *Mem. Geol. Soc. Jpn., 18,* 129-153, 1980.

Hyndman, R.D., K. Wang, and M. Yamano, Thermal constraints on the seismogenic portion of the southwestern Japan subduction thrust, *J. Geophys. Res., 100,* 15,373-15,392, 1995.

Ishibashi, K., The 1995 Kobe, Japan, earthquake (M7.1) in the "Amurian Plate Eastern Margin Mobile Belt" and its implication to the regional seismic activity (Preliminary) (in Japanese), *Chishitsu News, 490,* 14-21, 1995.

Ishida, M., Geometry and relative motion of the Philippine Sea plate and Pacific plate beneath the Kanto-Tokai district, Japan, *J. Geophys. Res., 97,* 489-513, 1992.

Ishikawa, N., and M. Hashimoto, Average horizontal crustal strain in Japan during interseismic period deduced from geodetic surveys (part 2) (in Japanese with English abstract), *Zisin, 52,* 299-315, 1999.

Ito, T., S. Yoshioka, and S. Miyazaki, Interplate coupling in southwest Japan deduced from inversion analysis of GPS data, *Phys. Earth Planet. Inter., 115,* 17-34, 1999.

Jackson, D.D., The use of a priori data to resolve nonuniqueness in linear inversion, *J. Geophys. J. R. Astron. Soc., 57,* 137-157, 1979.

Jackson, D.D., and M. Matsu'ura, A Bayesian approach to nonlinear inversion, *J. Geophys. Res., 90,* 581-591, 1985.

Kato, T., G.S. El-Fiky, E.N. Oware, and S. Miyazaki, Crustal strains in Japanese islands as deduced from dense GPS array, *Geophys. Res. Lett., 25,* 3445-3448, 1998a.

Kato, T., et al., Initial results from WING, the continuous GPS network in the western Pacific area, *Geophys. Res. Lett., 25,* 369-372, 1998b.

Kikuchi, M. and H. Kanamori, Rupture process of the Kobe, Japan, Earthquake of Jan. 17, 1995, determined from teleseismic body waves, *J. Phys. Earth, 44,* 429-436, 1996.

Kobayashi, Y., Initiation of subduction of plates (in Japanese), *Earth Mon., 5,* 510-514, 1983.

Kotake, Y., T. Kato, S. Miyazaki, and A. Sengoku, Relative motion of the Philippine Sea plate derived from GPS observations and tectonics of south-western Japan (in Japanese with English abstract), *Zisin, 51,* 171-180, 1998.

Kumagai, H., Time sequence and the recurrence models for large earthquakes along the Nankai Trough revisited, *Geophys. Res. Lett., 23,* 1139-1142, 1996.

Larson, K.M., R. Burgmann, R. Bilham, and J. Freymueller, Kinematics of the India-Eurasia collision zone from GPS measurements, *J. Geophys. Res., 104,* 1077-1093, 1999.

Mao, A., C.G.A. Harrison, and T.H. Dixon, Noise in GPS coordinate time series, *J. Geophys. Res., 104,* 2797-2816, 1999.

Matsu'ura, M., D.D. Jackson, and A. Cheng, Dislocation model for aseismic crustal deformation at Hollister, California, *J. Geophys. Res., 91,* 12,661-12,674, 1986.

Mazzotti, S., X. Le Pichon, P. Henry, and S. Miyazaki, Full interseismic locking of the Nankai and Japan-West Kurile subduction zones: An analysis of uniform elastic strain accumulation in Japan constrained by permanent GPS, *J. Geophys. Res., 105,* 13,159-13,177, 2000.

Miyazaki, S., T. Saito, M. Sasaki, Y. Hatanaka, and Y. Iimura, Expansion of GSI's nationwide GPS array, *Bull. Geogr. Surv. Inst., 43,* 23-34, 1997.

Mogi, K., Some features of recent seismic activity in and near Japan, 2, Activity before and after great earthquakes, *Bull. Earthquake Res. Inst., 47,* 395-417, 1969.

Molnar, P., and J.M. Gipson, A bound on the rheology of continental lithosphere using very long baseline interferometry: The velocity of south China with respect to Eurasia, *J. Geophys. Res., 101,* 545-553, 1996.

Molnar, P., and P. Tapponnier, Cenozoic tectonics of Asia: Effects of a continental collision, *Science, 189,* 419-426, 1975.

Nakamura, K., Possible nascent trench along the eastern margin Japan Sea as the convergence boundary between Eurasian and North American plates (in Japanese with English abstract), *Bull. Earthquake Res. Inst., 58,* 711-722, 1983.

Nishimura, S., M. Ando, and S. Miyazaki, Inter-plate coupling along the Nankai Trough and southeastward motion along southern part of Kyushu (in Japanese with English abstract), *Zisin, 51,* 443-456, 1999.

Nishimura, T., et al., Distribution of seismic coupling on the subducting plate boundary in northeastern Japan inferred from GPS observation, *Tectonophysics, 323,* 217-238, 2000.

Okada, A., On the Quaternary faulting along the Median Tectonic Line, in *Median Tectonic Line* (in Japanese with English abstract), edited by R. Sugiyama, pp. 49-86, Tokai Univ. Press, Tokyo, 1973.

Okada, Y., Internal deformation due to shear and tensile faults in a half-space, *Bull. Seismol. Soc. Am., 82,* 1018-1040, 1992.

Okano, K., S. Kimura, T. Konomi, and M. Nakamura, The focal distribution of earthquakes in Shikoku and its surrounding regions (in Japanese with English abstract), *Zisin, 38,* 93-103, 1985.

Ozawa, T., T. Tabei, and S. Miyazaki, Interplate coupling along the Nankai Trough off southwest Japan derived from GPS measurements, *Geophys. Res. Lett., 26,* 927-930, 1999.

Sagiya, T., Crustal deformation cycle and interplate coupling in Shikoku, southwest Japan, Ph.D. thesis, 164 pp., Univ. of Tokyo, Tokyo, 1995.

Sagiya, T., and W. Thatcher, Coseismic slip resolution along a plate boundary megathrust: The Nankai Trough, southwest Japan, *J. Geophys. Res., 104,* 1111-1129, 1999.

Sangawa, A., The paleo-earthquake study using traces of the liquefaction (in Japanese), *Quat. Res., 32,* 249-255, 1993.

Savage, J.C., A dislocation model of strain accumulation and release at a subduction zone, *J. Geophys. Res., 88,* 4984-4996, 1983.

Schulz, S.S., G.M. Mavko, R.O. Burford, and W.D. Stuart, Longterm fault creep observations in central California, *J. Geophys. Res., 87,* 6977-6982, 1982.

Seno, T., S. Stein, and A.E. Gripp, A model for the motion of the Philippine Sea Plate consistent with Nuvel 1 and geological data, *J. Geophys. Res., 98,* 17,941-17,948, 1993.

Sibuet, J.-C., B. Deffontaines, S.-K. Hsu. N. Thareau, J.-P. Le Formal, C.-S. Liu, and ACT party, Okinawa trough backarc basin: Early tectonic and magmatic evolution, *J. Geophys. Res., 103,* 30,245-30,267, 1998.

Sillard, P., Z. Altamimi, and C. Boucher, The ITRF96 realization and its associated velocity field, *Geophys. Res. Lett., 25,* 3223-3226, 1998.

Tabei, T. et al, Dense GPS observation across the Median Tectonic Line for detecting deep structure and current slip distribution, paper presented at the Seismological Society of Japan 1999 Fall Meeting, Seismol. Soc. of Jpn., Sendai, Miyagi, Japan, Nov. 17-19, 1999.

Tada, T., Spreading of the Okinawa trough and its relation to the crustal deformation in Kyushu (in Japanese with English abstract), *Zisin, 37,* 407-415, 1984.

Tada, T., Spreading of the Okinawa trough and its relation to the crustal deformation in Kyushu, Part 2 (in Japanese with English abstract), *Zisin, 38,* 1-12, 1985.

Thatcher, W., The earthquake deformation cycle at the Nankai Trough, southwest Japan, *J. Geophys. Res., 89,* 3087-3101, 1984.

Tsuji, H., Y. Hatanaka, T. Sagiya, and M. Hashimoto, Coseismic crustal deformation from the 1994 Hokkaido-Toho-Oki earthquake monitored by a nationwide continuous GPS array in Japan, *Geophys. Res. Lett., 22,* 1669-1672, 1995.

Wang, K., Stress-strain "paradox," plate coupling, and forearc seismicity at the Cascadia and Nankai subduction zones, *Tectonophysics,* in press, 2000.

Wei, D.-P., and T. Seno, Determination of the Amurian plate motion, in *Mantle Dynamics and Plate Interactions in East Asia, Geodyn. Ser.,* vol. 27, edited by M.F.J. Flower et al., pp. 337-346, AGU, Washington D. C., 1998.

Yabuki, T., and M. Matsu'ura, Geodetic data inversion using a Beyesian information criterion for spatial distribution of fault slip, *Geophys. J. Int., 109,* 363-375, 1992.

Zhang, J., Y. Bock, H. Johnson, P. Fang, S. Williams, J. Genrich, S. Wdowinski, and J. Behr, Southern California Permanent GPS Geodetic Array: Error analysis of daily position estimates and site velocities, *J. Geophys. Res., 102,* 18,035-18,055, 1997.

Zonenshain, L.P., and L.A. Savostin, Geodynamics of the Baikal rift zone and plate tectonics of Asia, *Tectonophysics, 76,* 1-45, 1981.

K. Heki, Division of Earth Rotation, Mizusawa Astrogeodynamics Observatory, National Astronomical Observatory, 2-12 Hoshigaoka, Mizusawa-city, Iwate 023-0861, Japan. (heki@miz.nao.ac.jp)

S. Miyazaki, Geography and Crustal Dynamics Research Center, Geographical Survey Institute, Kitasato-1, Tsukuba, Ibaraki, 305-0811, Japan. (miyazaki@gsi-mc.go.jp)

(Received January 7, 2000; revised July 6, 2000;
accepted August 14, 2000.)